Inorganic Chemistry

Article

Cite This: Inorg. Chem. XXXX, XXX, XXX−XXX

pubs.acs.org/IC

cis-Dioxorhenium(V/VI) Complexes Supported by Neutral Tetradentate N_4 Ligands. Synthesis, Characterization, and Spectroscopy

Vicky Yin-Ming Ng,[†,∥] Chun-Wai Tse,[†,∥] Xiangguo Guan,[†] Xiaoyong Chang,[†] Chen Yang,[†] Kam-Hung Low,[†] Hung Kay Lee,[‡] Jie-Sheng Huang,[†] and Chi-Ming Che*[,†,§]

[†]State Key Laboratory of Synthetic Chemistry, Institute of Molecular Functional Materials, and Department of Chemistry, The University of Hong Kong, Pokfulam Road, Hong Kong, People's Republic of Chinaa

[‡]Department of Chemistry, The Chinese University of Hong Kong, New Territories, Hong Kong, People's Republic of China

[§]HKU Shenzhen Institute of Research and Innovation, Shenzhen 518053, People's Republic of China

Supporting Information

ABSTRACT: A series of *cis*-dioxorhenium(V) complexes containing chiral tetradentate N_4 ligands, including *cis*-$[Re^V(O)_2(pyxn)]^+$ (**1**; pyxn = *N*,*N*′-dimethyl-*N*,*N*′-bis(2-pyridylmethyl)cyclohexane-1,2-diamine), *cis*-$[Re^V(O)_2(6\text{-}Me_2pyxn)]^+$ (***cis*-2**), *cis*-$[Re^V(O)_2(R,R\text{-}pdp)]^+$ (**3**; *R*,*R*-pdp = 1,1′-bis((*R*,*R*)-2-pyridinylmethyl)-2,2′-bipyrrolidine), *cis*-$[Re^V(O)_2(R,R\text{-}6\text{-}Me_2pdp)]^+$ (**4**), and *cis*-$[Re^V(O)_2(bqcn)]^+$ (**5**; bqcn = *N*,*N*′-dimethyl-*N*,*N*′-di(quinolin-8-yl)cyclohexane-1,2-diamine), were synthesized. Their structures were established by X-ray crystallography, showing Re−O distances in the range of 1.740(3)−1.769(8) Å and O−Re−O angles of 121.4(2)−124.8(4)°. Their cyclic voltammograms in MeCN (0.1 M $[NBu_4]PF_6$) display a reversible $Re^{VI/V}$ couple at $E_{1/2}$ = 0.39−0.49 V vs SCE. In aqueous media, three proton-coupled electron transfer reactions corresponding to $Re^{VI/V}$, $Re^{V/III}$, and $Re^{III/II}$ couples were observed at pH 1. The Pourbaix diagrams of **1**·OTf, **3**·OTf, and **5**·OTf have been examined. The electronic absorption spectra of the *cis*-dioxorhenium(V) complexes show three absorption bands at around 800 nm (600−1730 $dm^3\ mol^{-1}\ cm^{-1}$), 580 nm (1700−5580 $dm^3\ mol^{-1}\ cm^{-1}$), and 462−523 nm (3170−6000 $dm^3\ mol^{-1}\ cm^{-1}$). Reaction of **1** with Lewis acids (or protic acids) gave *cis*-$[Re^V(O)(OH)(pyxn)]^{2+}$ (**1**·H^+), in which the Re−O distances are lengthened to 1.788(5) Å. Complex ***cis*-2** resulted from isomerization of ***trans*-2** at elevated temperature. *cis*-$[Re^{VI}(O)_2(pyxn)](PF_6)_2$ (**1′**·$(PF_6)_2$) was obtained by constant-potential electrolysis of **1**·PF_6 in MeCN (0.1 M $[NBu_4]PF_6$) at 0.56 V vs SCE; it displays shorter Re−O distances (1.722(4), 1.726(4) Å) and a smaller O−Re−O angle (114.88(18)°) relative to **1** and shows a d−d transition absorption band at 591 nm (ε = 77 $dm^3\ mol^{-1}\ cm^{-1}$). With a driving force of ca. 75 kcal mol^{-1}, **1′** oxidizes hydrocarbons with weak C−H bonds (75.5−76.3 kcal mol^{-1}) via hydrogen atom abstraction. DFT and TDDFT calculations on the electronic structures and spectroscopic properties of the *cis*-dioxorhenium(V/VI) complexes were performed.

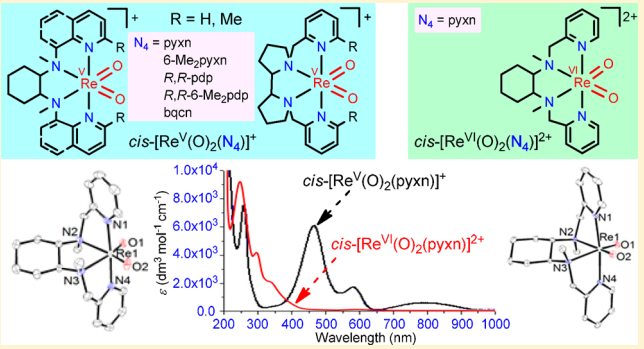

INTRODUCTION

cis-Dioxo metal complexes constitute an important class of compounds in metal-catalyzed oxidation reactions,[1,2a−h] with an exemplary example being alkene cis-dihydroxylation involving the [3 + 2] cycloaddition pathway.[2a,h] For d^2 dioxo systems, the trans configuration is more stable. The cis configuration is generally favored in d^0 and d^1 dioxo systems to maximize π-bonding interactions between dπ(metal) and pπ(O) orbitals. A large number of *trans*-dioxo d^2 metal complexes[1,2b,i,j,3−10] have been studied; a notable example with Re(V) ion is *trans*-$[Re^V(O)_2(py)_4]^+$ (py = pyridine), which has been demonstrated to show interesting spectroscopic and photophysical properties by Gray and co-workers.[4] *cis*-Dioxo d^2 metal complexes have been less explored, particularly for octahedral ones, examples of which that have been characterized structurally and/or spectroscopically include Os(VI)[11,12] and Ru(VI) complexes[13,14] as well as limited examples of Re(V) complexes: *cis*-$[Re^V(O)_2(bpy)(py)_2]^+$,[15] *cis*-$[Re^V(O)_2(Me_3tacn)(OH_2)]^+$,[16] and *cis*-$[Re^V(O)_2(Hdab)(py)_2]$[17] (bpy = 2,2′-bipyridine; Me_3tacn = *N*,*N*′,*N*″-trimethyl-1,4,7-triazacyclononane; H_2dab = 1,2-diaminobenzene). We[18b] and Meyer[18a] also reported electrochemical generation of *cis*-dioxo d^2 metal complexes of Ru and/or Os from the *cis*-$M(OH_2)_2$ (M = Ru, Os) precursors.

cis-Dioxo d^1 metal complexes are even sparse in the literature, with limited examples belonging to Cr(V)[19] and Mo(V) complexes,[20] together with two types of Re(VI) complexes: *cis*-

Received: September 19, 2017

DOI: 10.1021/acs.inorgchem.7b02404
Inorg. Chem. XXXX, XXX, XXX−XXX

$[Re^{VI}(O)_2(Ar)_2]$ (Ar = xylyl, mesityl)[21] and *cis*-$[(Tp)Re^{VI}(O)_2(X)]$ (Tp = hydrotris(pyrazol-1-yl)borate; X = Cl^-, Br^-, I^-)[22] bearing mono- and/or tridentate ligands. Notably, *cis*-$[Re^{VI}(O)_2(Ar)_2]$ adopts a tetrahedral geometry; complexes *cis*-$[(Tp)Re^{VI}(O)_2(X)]$ represent the only examples of octahedral d^1 *cis*-dioxorhenium(VI) complexes known to date.

The structurally characterized *cis*-dioxorhenium(V) complexes reported so far bear mono-, bi-, and/or tridentate ligands,[15−17,23−27] including the octahedral complexes mentioned above[15−17] and the five-coordinate complexes *cis*-$[Re^{V}(O)_2I(PPh_3)_2]$,[24] *cis*-$[Re^{V}(O)_2Me(PhC{=}CPh)]$,[25] *cis*-$[Re^{V}(O)_2(R_2NCH_2CH_2S)(PPh_3)]$ (R_2N = $(OCH_2CH_2O)C(CH_2CH_2)_2N$),[26a] Et_2N,[26b] (*o*-$MeOC_6H_4$)$N(CH_2CH_2)_2N$[26b]), and *cis*-$[Re^{V}(O)_2Me(PR_3)_2]$ (R = Ph, Cy).[27] There is one report on a *cis*-dioxorhenium(V) complex containing a tetradentate ligand. Reaction of *cis*-$[Re^{V}(O)_2I(PPh_3)_2]$ with an achiral neutral tetradentate ligand, 1,4,7,10-tetrazacyclododecane (cyclen), was reported to give octahedral *cis*-$[Re^{V}(O)_2(cyclen)]^+$ on the basis of ^1H NMR analysis; however, this complex has not been characterized by X-ray crystal analysis and could not be isolated in pure form.[28] In contrast to the structures of *cis*-dioxorhenium(V) complexes, their spectroscopy has been much less studied. *cis*-$[Re^{V}(O)_2(bpy)(py)_2]^+$ and its derivatives display an electronic absorption band at about 490 nm (ε = 4200−4600 $dm^3\ mol^{-1}\ cm^{-1}$) that was tentatively assigned to MLCT transitions.[15b,c] *cis*-$[Re^{V}(O)_2(Me_3tacn)(OH_2)]^+$ was only mentioned to show a low-energy d−d absorption band at ca. 680 nm.[16] A quest remains to explore the spectroscopy of *cis*-dioxorhenium(V) complexes and to compare it with that of *trans*-dioxo complexes.[4,6c]

We are interested in studying the chemistry of cis-metal complexes supported by tetradentate N_4 ligands. In the literature, there are a considerable number of iron and manganese complexes supported by the neutral N_4 ligands pyxn, pdp, and bqcn (and their substituted forms) that have been reported to catalyze various oxidation reactions[29−31] (pyxn = *N*,*N*′-dimethyl-*N*,*N*′-bis(2-pyridylmethyl)cyclohexane-1,2-diamine; pdp = 1,1′-bis(2-pyridinylmethyl)-2,2′-bipyrrolidine; bqcn = *N*,*N*′-dimethyl-*N*,*N*′-bis(quinolin-8-yl)-cyclohexane-1,2-diamine). Reactive chiral *cis*-$[M(O)_2(N_4)]^{n+}$ species, such as *cis*-$[Mn^{V}(O)_2(S,S\text{-bqcn})]^+$,[31b] have been suggested to play an important role in the asymmetric oxidation reaction; however, the isolation and characterization of *cis*-$[M(O)_2(S,S\text{-bqcn})]^{n+}$ have not been reported. As high-valent Re complexes[15−17] are considerably less oxidizing, *cis*-$[Re^{V}(O)_2(N_4)]^+$ complexes are likely to be stable and isolable; fundamental studies on these complexes can provide grounds for further investigation on the structure of the putative reactive chiral *cis*-$[M(O)_2(N_4)]^{n+}$ species bearing the same chiral N_4 ligand in the Fe and Mn oxidation chemistry.

In this present work, a series of *cis*-dioxorhenium(V) complexes and also a *cis*-dioxorhenium(VI) complex bearing chiral tetradentate N_4 ligands, that is, *cis*-$[Re^{V}(O)_2(N_4)]^+$ (N_4 = pyxn (**1**), 6-Me_2pyxn (***cis*-2**), *R*,*R*-pdp (**3**), *R*,*R*-6-Me_2pdp (**4**), bqcn (**5**)) and *cis*-$[Re^{VI}(O)_2(pyxn)]^{2+}$ (**1′**), were synthesized (Chart 1) and structurally characterized by X-ray crystal analysis; their electrochemistry and electronic absorption spectra were examined. The complex *cis*-$[Re^{VI}(O)_2(pyxn)]^{2+}$ (**1′**) was obtained by electrochemical oxidation of *cis*-$[Re^{V}(O)_2(pyxn)]^{2+}$ (**1**); the two complexes bearing the same pyxn ligand allow a direct comparison between octahedral *cis*-$Re^{VI}(O)_2$ and *cis*-$Re^{V}(O)_2$ complexes (in the case of $[(Tp)Re^{VI}(O)_2(X)]$,[22] the *cis*-$Re^{V}(O)_2$ counterpart has not been reported). The acid−base chemistry of **1** and its implication on the electronic structure are discussed. Notably, for $[Re^{V}(O)_2(6\text{-}Me_2pyxn)]^+$ (**2**), both its cis and trans isomers have been obtained, allowing a direct comparison of the structural and spectroscopic properties between *cis*- and *trans*-dioxorhenium(V) complexes having the same auxiliary ligands. DFT and TDDFT calculations were performed to analyze the electronic structure and spectroscopic data of these structurally characterized, chiral N_4 ligand supported, octahedral *cis*-dioxorhenium(V/VI) complexes.

Chart 1. Structures of Dioxorhenium Complexes 1, 3−5, 1′, and *cis*- and *trans*-2 in This Work

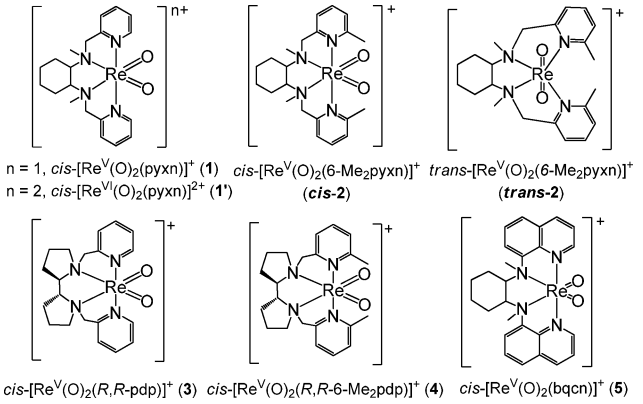

RESULTS

Synthesis and Characterization. Reactions of *cis*-$[Re^{V}(O)_2(PPh_3)_2I]$ with the corresponding N_4 ligand in dichloromethane afforded *cis*-$[Re^{V}(O)_2(pyxn)]^+$ (**1**) and *cis*-$[Re^{V}(O)_2(R,R\text{-pdp})]^+$ (**3**) in 16% and 30% yields, respectively. *trans*-$[Re^{V}(O)_2(6\text{-}Me_2pyxn)]^+$ (***trans*-2**), *cis*-$[Re^{V}(O)_2(R,R\text{-}6\text{-}Me_2pdp)]^+$ (**4**), and *cis*-$[Re^{V}(O)_2(bqcn)]^+$ (**5**) were synthesized in yields of 13%, 4%, and 3%, respectively, using another procedure, in which a tetrahydrofuran solution of *cis*-$[Re^{V}(O)_2(PPh_3)_2I]$ and the corresponding N_4 ligand was refluxed under argon for 2 h. *cis*-$[Re^{V}(O)_2(6\text{-}Me_2pyxn)]PF_6$ (***cis*-2**·PF_6) was obtained by refluxing ***trans*-2**·PF_6 in acetonitrile for 4 h, followed by recrystallization, in 48% yield. *cis*-$[Re^{VI}(O)_2(pyxn)](PF_6)_2$ (**1′**·$(PF_6)_2$) was prepared by constant-potential electrolysis of *cis*-$[Re^{V}(O)_2(pyxn)]PF_6$ (**1**·PF_6) in MeCN (0.1 M$[NBu_4]PF_6$) at 0.56 V vs SCE. *cis*-$[Re^{V}(O)(OH)(pyxn)]^{2+}$ (**1**·H^+) was obtained from the reaction of **1** with Lewis acids (or protic acids). These complexes were characterized by MS (+ESI), IR and elemental analyses. The Re(V) complexes **1**−**5** are diamagnetic and show well-resolved ^1H and ^{13}C NMR spectra (Figures S1−S5 in the Supporting Information). Complexes **3** and **4** bearing *R*,*R*-pdp and *R*,*R*-6-Me_2pdp ligands, respectively, were characterized by circular dichroism spectroscopy (Figure S6 in the Supporting Information). Complex **1′** is paramagnetic with a measured magnetic moment of μ_{eff} = 1.72 μ_B,[32] which is consistent with a d^1 electronic configuration.[19b,22,33,34] The EPR spectrum of **1′** at 7 K shows multiple lines with a simulated *g* value of 1.93 (Figure S7 in the Supporting Information).

The infrared (IR) spectra of *cis*-$[Re^{V}(O)_2]^+$ complexes (**1**, ***cis*-2**, and **3**−**5** as ClO_4^- salts except for **4**·BPh_4) reveal two absorption bands at 910−930 and 880−890 cm^{-1}, which are attributed to the symmetric and asymmetric ν(O−Re−O)

DOI: 10.1021/acs.inorgchem.7b02404
Inorg. Chem. XXXX, XXX, XXX−XXX

stretches, respectively. The $\nu_{sym}(ReO_2)$ stretches are comparable to those of *cis*-$[Re^V(O)_2(bpy)(py)_2]^+$ (904 cm^{-1})[15b] and *cis*-$[Re^V(O)_2(Hdab)(py)_2]$ (905 cm^{-1}).[17] *trans*-$[Re^V(O)_2(6\text{-}Me_2pyxn)]PF_6$ (***trans*-2**·PF_6) displays an IR absorption band at 785 cm^{-1} corresponding to an asymmetric *trans*-$[Re^V(O)_2]^+$ stretch, similar to that reported for *trans*-$[Re^V(O)_2(diphosphine)_2]^+$ (784.8−786.3 cm^{-1}).[8b] The ^1H NMR spectra of **1**, ***cis*-2**, and **3**−**5** (as PF_6 salt except for **4**·BPh_4) exhibit aromatic signals at 7−8 ppm (pyridyl/quinolyl), doublet of doublets/singlet signals at 6−6.7 ppm (bridging CH_2), and aliphatic signals at 0.7−4 ppm (Cy/bipyrrolidyl) (see Figures S1−S4 in the Supporting Information). The N−CH_3 protons of **1**, ***cis*-2**, and **5** contribute to the sharp singlet peaks at 3.3−4.4 ppm, whereas the 6-methyl protons on the pyridyl groups of ***cis*-2** and **4** appear as singlet peaks at ∼2.7 ppm. The ^1H NMR spectrum of ***trans*-2**·PF_6 displays three sets of aromatic signals at 7.5−8 ppm (pyridyl), two doublets at 5.2−5.7 ppm (bridging CH_2), one singlet at 2.87 ppm (NCH_3), another singlet at 2.55 ppm (6-CH_3py), and aliphatic signals at 1.2−4.1 ppm (Cy) (Figure S5 in the Supporting Information). On comparison of ***trans*-2** and ***cis*-2**, the three sets of aromatic signals with an integral ratio of 1:1:1 in ***trans*-2** convert into two sets with an integral ratio of 2:1 in ***cis*-2**. The bridging CH_2 protons of ***trans*-2** (5.2−5.7 ppm) are less deshielded than that of ***cis*-2** (6−6.2 ppm). On the other hand, the N−C(Cy)−H proton signal of ***trans*-2** (4.05 ppm) is much more deshielded than that of ***cis*-2** (2.05 ppm). Insignificant differences were observed when the ^1H NMR spectra of freshly dissolved ***cis*-2**·PF_6 or ***trans*-2**·PF_6 were recorded at 60 °C.

The *cis*-$[Re^V(O)_2(N_4)]^+$ complexes are stable in the solid state for months and in acetonitrile solution for days, while ***trans*-2** undergoes isomerization to ***cis*-2** thermally. Time-dependent ^1H NMR spectroscopy revealed that ***trans*-2**·PF_6 slowly isomerizes into ***cis*-2**·PF_6 after standing in acetonitrile solution at room temperature in the dark (Figure 1), during

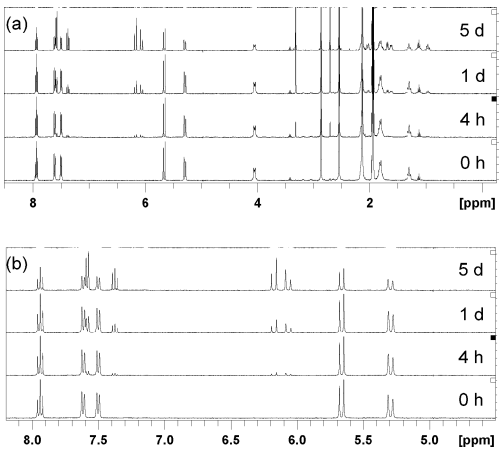

Figure 1. Changes in the regions of (a) −0.5 to +8.5 ppm and (b) 4.5−8.2 ppm in the ^1H NMR spectra of ***trans*-2**·PF_6 in MeCN-d_3 solution at room temperature.

which a color change from yellow to brown was observed. The kinetics and thermodynamics of the isomerization of ***trans*-2** to ***cis*-2** was followed by UV−vis spectroscopy. Figure 2 depicts the spectral changes when a solution of ***trans*-2** was incubated at 50 °C in acetonitrile, showing the depletion of ***trans*-2** and clean formation of ***cis*-2** with an isosbestic point at 385 nm. The time-dependent total concentration of ***trans*-2** and ***cis*-2**

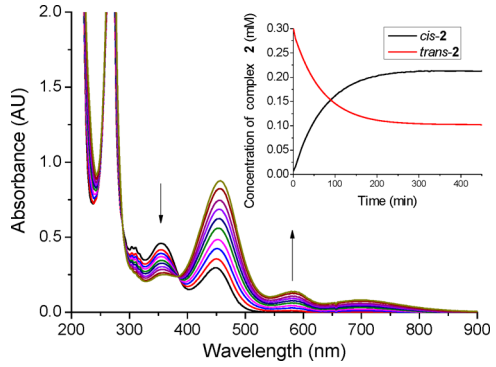

Figure 2. UV−vis spectral changes over 6 h of an acetonitrile solution of ***trans*-2** (3×10^{-4} M) incubated at 50 °C. Inset: depletion of ***trans*-2** monitored at 355 nm and formation of ***cis*-2** monitored at 580 nm.

corresponds to the initial concentration of ***trans*-2**. A third species was not observed in either the UV−vis or ^1H NMR spectrum. After reaching equilibrium, the *cis*/*trans* ratio corresponds to an equilibrium constant (K_{eq}) of 2.09. Similarly, starting with ***cis*-2**, the same equilibrium ratio between the two isomers was reached after incubation at 50 °C for 6 h, suggesting the reversibility of the isomerization process. Analogous to other isomerization processes reported in the literature,[35] the *trans*-*cis* isomerization of **2** can be treated as a reversible first-order reaction:

$$\textbf{\textit{trans}-2} \underset{k_{c\text{-}t}}{\overset{k_{t\text{-}c}}{\rightleftharpoons}} \textbf{\textit{cis}-2} \qquad K_{eq} = \frac{[\textbf{\textit{cis}-2}]}{[\textbf{\textit{trans}-2}]}$$

The rates of the forward reaction ($k_{t\text{-}c}$) and backward reaction ($k_{c\text{-}t}$), and K_{eq} at different temperatures (40−70 °C) are summarized in Table 1. The experimental rate data were

Table 1. Rate and Equilibrium Constants for Trans−Cis Isomerization of 2 in Acetonitrile

temp (°C)	$k_{t\text{-}c}$ (10^{-4} s^{-1})	$k_{c\text{-}t}$ (10^{-4} s^{-1})	K_{eq}
40	0.49	0.23	2.11
50	1.67	0.80	2.09
60	6.17	2.98	2.07
70	19.59	9.51	2.06

used in conjunction with the Eyring equation (see Figure S8 and the Experimental Section in the Supporting Information for details) to calculate the activation enthalpy ($\Delta H^{‡}$) and entropy ($\Delta S^{‡}$) (Table 2). The Gibbs free energies ($\Delta G^{‡}$) at 50 °C (323

Table 2. Thermodynamic Activation Parameters for Trans−Cis Isomerization of 2 in Acetonitrile

$\Delta H^{‡}$ (kJ mol^{-1})		$\Delta S^{‡}$ (J K^{-1} mol^{-1})		$\Delta G^{‡}$(323 K) (kJ mol^{-1})	
t-c	c-t	t-c	c-t	t-c	c-t
107.7	108.7	16.0	12.8	102.7	104.7

K) were determined to be 102.7 kJ mol^{-1} (t-c) and 104.7 kJ mol^{-1} (c-t), respectively. The very small Gibbs free energy difference ($\Delta\Delta G^{‡}$) reveals that the stabilities of the cis isomer and corresponding trans isomer are comparable.

Crystal Structures. The structures of **1**, ***cis*-2**, ***trans*-2**, **3**−**5**, and **1′** were established by X-ray crystallography (Figures 3 and 5). Diffraction-quality crystals of *cis*-$[Re^V(O)_2(N_4)]^+$ (**1**, ***cis*-2**, and **3**−**5**; PF_6 anion except for **4**·BPh_4) were obtained by

DOI: 10.1021/acs.inorgchem.7b02404
Inorg. Chem. XXXX, XXX, XXX−XXX

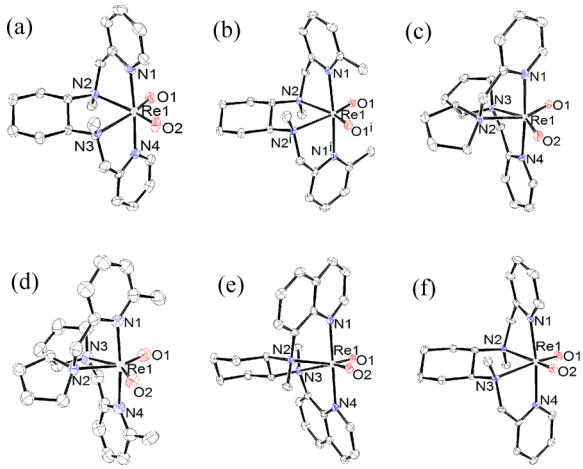

Figure 3. ORTEP drawings of (a) *cis*-$[Re^{V}(O)_2(pyxn)]^+$ (**1**), (b) *cis*-$[Re^{V}(O)_2(6\text{-}Me_2pyxn)]^+$ (***cis*-2**), (c) *cis*-$[Re^{V}(O)_2(R,R\text{-}pdp)]^+$ (**3**), (d) *cis*-$[Re^{V}(O)_2(R,R\text{-}6\text{-}Me_2pdp)]^+$ (**4**), (e) *cis*-$[Re^{V}(O)_2(bqcn)]^+$ (**5**), and (f) *cis*-$[Re^{VI}(O)_2(pyxn)]^{2+}$ (**1′**). Hydrogen atoms are not shown.

diffusion of diethyl ether into methanol solutions of the complexes. Selected bond distances and angles are given in Table 3. All of the *cis*-dioxorhenium(V) complexes adopt a pseudo-octahedral geometry with *cis*-α configuration. The Re−O distances are 1.740(3)−1.769(8) Å, which are close to the computed values (1.749−1.754 Å, Tables S9−S13 in the Supporting Information) in the DFT-optimized ground state (S_0) geometries. These Re−O distances fall within the range (1.716(6)−1.82(1) Å) of those reported for octahedral complexes *cis*-$[Re^{V}(O)_2(Hdab)(py)_2]$ (1.716(6), 1.723(7) Å),[17] *cis*-$[Re^{V}(O)_2(bpy)(py)_2]^+$ (1.733(8), 1.736(7) Å),[15a] and *cis*-$[Re^{V}(O)_2(OH_2)(Me_3tacn)]^+$ (1.78(1), 1.82(1) Å).[16] The experimental and computed O1−Re1−O2 bond angles (α in Figure 4) for *cis*-$[Re^{V}(O)_2(N_4)]^+$ (**1**, ***cis*-2**, and **3**−**5**) are 121.4−124.8 and 124.0−127.0°, respectively; both values are comparable to those of *cis*-$[Re^{V}(O)_2(bpy)(py)_2]^+$ (121(4)°)[15a] and *cis*-$[Re^{V}(O)_2(Hdab)(py)_2]$ (118.2(3)°)[17] but larger than that of *cis*-$[Re^{V}(O)_2(OH_2)(Me_3tacn)]^+$ (106.7(5)°).[16] In the cases of **1** and **3**, introducing methyl groups to the 6-position of their pyridyl groups to give ***cis*-2** and **4**, respectively, slightly increases the O−Re−O angle (α in Figure 4) (121.4(2) → 123.75(15)° for **1** → ***cis*-2**, 122.5(2) → 124.8(4)° for **3** → **4**), probably owing to the repulsion between the oxo ligand and the 6-methyl group. The N2−Re−N3 angles (β in Figure 4) of these *cis*-dioxorhenium(V) complexes are 73.5(3)−77.56(11)°,

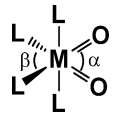

Figure 4. α and β angles in *cis*-dioxorhenium complexes.

while the corresponding angles of *cis*-$[Re^{V}(O)_2(bpy)(py)_2]^+$ and *cis*-$[Re^{V}(O)_2(Hdab)(py)_2]$ are 70.6(3)°[15a] and 72.7(3)°,[17] respectively. The experimental Re−N1 and Re−N4 distances are 2.101(3)−2.186(6) Å, which closely match with the computed values of 2.132−2.197 Å. The experimental N1−Re−N4 angles are 174.59(13)−179.71(13)°, which were also well reproduced by the computed values of 176.1−178.7°.

A crystal of *cis*-$[Re^{VI}(O)_2(pyxn)](PF_6)_2$ (**1′**·$(PF_6)_2$) suitable for X-ray diffraction analysis was obtained by slow diffusion of diethyl ether into an acetonitrile solution of **1′**·$(PF_6)_2$. The structure of **1′** is depicted in Figure 3f, which adopts a pseudo-octahedral geometry with cis-α configuration similar to that of **1**. In comparison to **1** (Re−O 1.750(5), 1.753(5) Å), the experimental Re−O distances of **1′** are slightly shorter (1.722(4), 1.726(4) Å; DFT-calculated 1.728 Å; Table S14 in the Supporting Information). These Re−O distances of **1′** are also slightly shorter than those of the octahedral complex *cis*-$[(Tp)Re^{VI}(O)_2(Cl)]$ (1.797(11) and 1.741(10) Å).[22] The experimental O−Re−O angle of 114.88(18)° (computed 116.5°, Table S14) of **1′** is smaller than that of **1** (121.4(2)°) but larger than that of *cis*-$[(Tp)Re^{VI}(O)_2(Cl)]$ (107.1(4)°).[22]

For *cis*-$[Re^{V}(O)(OH)(pyxn)](OTf)_2$ (**1**·H^+·$(OTf)_2$), a crystal suitable for X-ray diffraction analysis was obtained by slow diffusion of diethyl ether into an acetonitrile solution of **1** (12 mM) and $Sc^{III}(OTf)_3$ (6 mM) at 4 °C. In the unit cell, a C_2 axis passes through the Re center, which suggests disorder of the proton on the two oxo/hydroxo O atoms. In comparison to **1** (Re−O 1.750(5), 1.753(5) Å), the experimental Re−O distances of **1**·H^+ are slightly longer (1.788(5) Å); this is attributed to the weakening of Re−O π bonding by protonation. The experimental O−Re−O angle of 112.8(3)° of **1**·H^+ is significantly smaller than that of **1**. Notably, hydrogen bonding between the hydroxo group of **1**·H^+ and the N atom of cocrystallized acetonitrile is also observed (Figure S9 in the Supporting Information).

The X-ray crystal structure of *trans*-$[Re^{V}(O)_2(6\text{-}Me_2pyxn)]$-$ClO_4$ (***trans*-2**·ClO_4) is depicted in Figure 5. The Re−O distances are 1.768(4) Å, with a O−Re−O angle of 179.5(3)°. The Re−O distances are slightly longer than that of ***cis*-2**

Table 3. Selected Bond Distances (Å) and Angles (deg) of *cis*-Dioxorhenium Complexes, *cis*-$[Re^{V}(O)(OH)(pyxn)](OTf)_2$ (1·H^+·$(OTf)_2$), and *trans*-$[Re^{V}(O)_2(6\text{-}Me_2pyxn)]ClO_4$ (*trans*-2)

	1	*cis*-2[a]	3	4	5	1′	1·H^+[a]	*trans*-2[a]
Re−O1	1.750(5)	1.742(2)	1.765(4)	1.741(8)	1.740(3)	1.722(4)	1.788(5)	1.768(4)
Re−O2	1.753(5)	1.742(2)	1.749(4)	1.769(8)	1.752(3)	1.726(4)	1.788(5)	1.768(4)
Re−N1	2.121(6)	2.176(3)	2.122(5)	2.186(6)	2.101(3)	2.109(4)	2.097(6)	2.197(5)
Re−N4	2.124(6)	2.176(3)	2.132(5)	2.171(7)	2.105(3)	2.119(4)	2.097(6)	2.197(5)
Re−N2	2.275(5)	2.296(3)	2.258(5)	2.285(7)	2.291(3)	2.244(5)	2.232(5)	2.131(5)
Re−N3	2.276(6)	2.296(3)	2.252(4)	2.258(7)	2.284(3)	2.244(4)	2.232(5)	2.131(5)
O1−Re−O2 (α)	121.4(2)	123.75(15)	122.5(2)	124.8(4)	121.80(13)	114.88(18)	112.8(3)	179.5(3)
N1−Re−N4	175.6(2)	174.59(13)	176.3(2)	174.6(4)	179.71(13)	172.60(16)	174.1(3)	119.0(3)
N2−Re−N3 (β)	75.8(2)	74.41(14)	75.47(19)	73.5(3)	77.56(11)	77.00(15)	77.5(3)	87.3(3)

[a]O1[i], N2[i], and N1[i] atoms in the ORTEP drawings, which are generated by repeating the symmetric unit to form the whole structure, are presented as O2, N3, and N4 atoms, respectively.

DOI: 10.1021/acs.inorgchem.7b02404
Inorg. Chem. XXXX, XXX, XXX−XXX

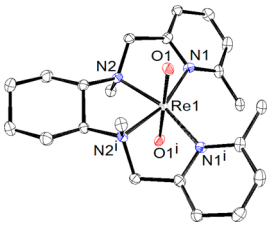

Figure 5. ORTEP drawing of *trans*-$[Re^{V}(O)_2(6\text{-}Me_2pyxn)]^+$ (***trans*-2**). Hydrogen atoms are not shown.

(1.742(2) Å) and are comparable to those of *trans*-$[Re^{V}(O)_2(py)_4]^+$ (1.745(12), 1.782(13) Å),[36] *trans*-$[Re^{V}(O)_2(en)_2]^+$ (1.761(7), 1.769(7) Å),[36] and $[Re^{V}(O)_2(diphosphine)_2]^+$ (1.748(4)–1.782(5) Å).[8b] The experimental Re–N1(py) and Re–N2(Cy) distances are 2.197(5) and 2.131(5) Å, respectively; the former is slightly longer than that of ***cis*-2** (2.176(3) Å), whereas the latter is much shorter than that of ***cis*-2** (2.296(3) Å). Notably, N1–Re–N4 angle of 119.0(3)° is much larger than 90.0° for an ideal octahedral geometry. In addition, ***trans*-2** (relative to ***cis*-2**) has a considerably larger N2–Re–N3 (β) angle (87.3(3) vs 74.41(14)°).

Electrochemistry. *In Nonaqueous Media.* The cyclic voltammograms of the *cis*-dioxorhenium(V) complexes in acetonitrile (0.1 M $[NBu_4]PF_6$) display a reversible oxidation couple at $E_{1/2}$ = 0.39–0.49 V vs SCE and an irreversible reduction wave at E_{pc} = −1.21 to −1.74 V vs SCE (Figure 6a and Table 4). The oxidation is attributable to a $Re^{VI/V}$ couple, the potentials of which are less anodic than that of *cis*-$[Re^{V}(O)_2(bpy)(py)_2]^+$ (0.77 V vs SCE).[15c] The reduction wave at E_{pc} = −1.21 to −1.74 V vs SCE is likely to be ligand-based reduction, since the E_{pc} of **5** is much less cathodic than that of **1**, ***cis*-2**, **3**, and **4** as a result of the replacement of pyridyl by the more conjugating quinolyl.

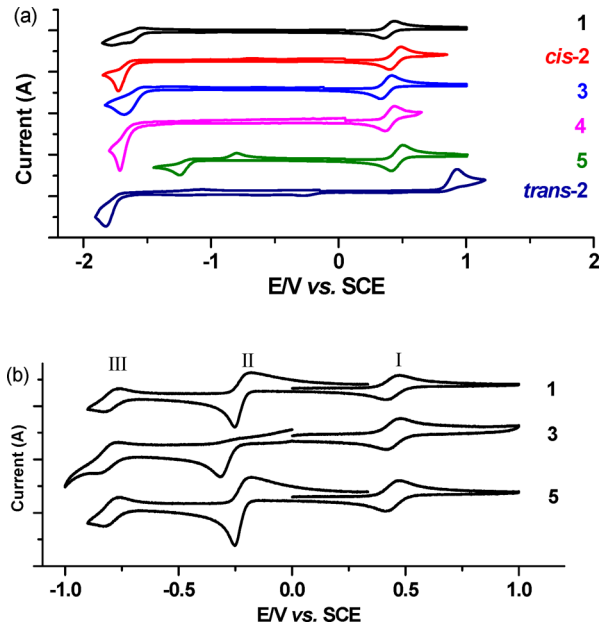

Figure 6. Cyclic voltammograms of (a) *cis*-dioxorhenium(V) complexes in acetonitrile (0.1 M $[NBu_4]PF_6$) and (b) *cis*-$[Re^{V}(O)_2(pyxn)]OTf$ (**1**·OTf), *cis*-$[Re^{V}(O)_2(R,R\text{-}pdp)]OTf$ (**3**·OTf), and *cis*-$[Re^{V}(O)_2(bqcn)]OTf$ (**5**·OTf) in 0.1 M CF_3SO_3H. Scan rate: 100 mV s^{-1}.

Table 4. Electrochemical Data of *cis*-Dioxorhenium(V) Complexes, $1\cdot H^+$, and *trans*-2 in Acetonitrile (0.1 M $[NBu_4]PF_6$)[a]

	E (V vs SCE)	
complex	reduction (E_{pc})	oxidation ($E_{1/2}$)
1	−1.74	0.42
***cis*-2**	−1.70	0.47
3	−1.67	0.39
4	−1.69	0.42
5	−1.21	0.49
***trans*-2**	−1.80	0.96[b]
$\mathbf{1}\cdot H^+$	−1.60	0.95[c]

[a]In acetonitrile with 0.1 M $[NBu_4]PF_6$ as the electrolyte. Glassy carbon was the working electrode, saturated calomel electrode (SCE) was the reference electrode, and platinum wire was the counter electrode. $E_{1/2}[(Me_5Cp)_2Fe^{+/0}]$ = −0.11 V vs SCE. [b]E_{pa} of the irreversible wave is reported. [c]The forward wave is broad with $E_{pa} \approx$ 1.3 V.

The cyclic voltammogram of *trans*-$[Re^{V}(O)_2(6,6'\text{-}Me_2pyxn)]PF_6$ (***trans*-2**·PF_6) in MeCN (0.1 M $[NBu_4]PF_6$) exhibits an irreversible oxidation wave at E_{pa} = 0.96 V vs SCE and an irreversible reduction wave at E_{pc} = −1.80 V vs SCE (Figure 6a). The oxidation wave is tentatively assigned to oxidation of Re^{V} to Re^{VI}, the potential of which is less anodic that that of *trans*-$[Re^{V}(O)_2(tmen)_2]^{+}$[8d] ($E_{1/2}$ = 1.41 V vs SCE, Figure S17 in the Supporting Information; tmen = *N*,*N*,*N*′,*N*′-tetramethylethylenediamine) and *trans*-$[Re^{V}(O)_2(dmpe)_2]^{+}$[8c] ($E_{pa}$ = 1.53 V vs SCE, Figure S17; dmpe = 1,2-bis(dimethylphosphino)ethane). The $E_{pa}(Re(V) \rightarrow Re(VI))$ value of ***trans*-2** is more anodic than the $E_{1/2}(Re^{VI/V})$ value of *cis*-$[Re^{V}(O)_2(N_4)]^+$ complexes by ca. 0.5 V. Presumably, *cis*-dioxo d^1 complexes are stabilized by additional π interaction between $d\pi(Re)$ and $p\pi(O)$ orbitals. The irreversible reduction wave of ***trans*-2** is ascribed to a ligand-based reduction, as the reduction potential is similar to that of **1** and ***cis*-2** (E_{pc} = −1.74 and −1.70 V vs SCE, respectively).

The cyclic voltammogram of *cis*-$[Re^{V}(O)(OH)(pyxn)](OTf)_2$ ($\mathbf{1}\cdot H^+\cdot(OTf)_2$) in MeCN (0.1 M $[NBu_4]PF_6$) shows distinct features in comparison to those of **1**. A broad oxidation wave was observed at a highly anodic potential ($E_{pa} \approx$ 1.3 V vs SCE), ascribable to the oxidation of $\mathbf{1}\cdot H^+$ (Figure 7). Interestingly, $\mathbf{1}\cdot H^+$ exhibits an additional reversible reduction couple at −0.31 V vs SCE that is tentatively attributed to one-electron reduction of $\mathbf{1}\cdot H^+$ to *cis*-$[Re^{IV}(O)(OH)(pyxn)]^+$. The ligand-based reduction of $\mathbf{1}\cdot H^+$ occurs at a slightly less cathodic potential relative to **1** (Table 4).

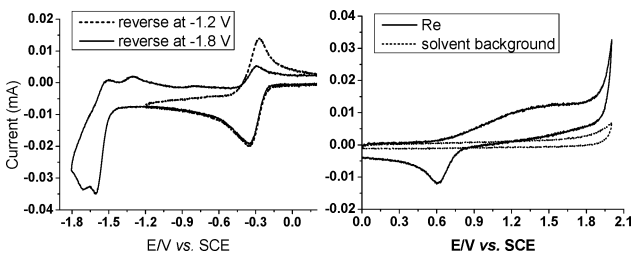

Figure 7. Cyclic voltammograms of *cis*-$[Re^{V}(O)(OH)(pyxn)](OTf)_2$ ($\mathbf{1}\cdot H^+\cdot(OTf)_2$) in acetonitrile (0.1 M $[NBu_4]PF_6$). Scan rate: 100 mV s^{-1}.

DOI: 10.1021/acs.inorgchem.7b02404
Inorg. Chem. XXXX, XXX, XXX–XXX

In Aqueous Media. Variable pH electrochemistry of *cis*-dioxorhenium(V) complexes in aqueous media has been conducted. At pH 1, complexes **1**·OTf, **3**·OTf, and **5**·OTf show a reversible oxidation couple at $E_{1/2}$ = 0.44−0.47 V vs SCE (couple I) and two reduction couples at around E = −0.20 to −0.32 V and −0.70 to −0.83 V vs SCE (couples II and III, respectively) (Figure 6b and Table 5). The current magnitude

Table 5. Electrochemical Data of *cis*-Dioxorhenium(V) Complexes in Aqueous Medium at Selected pH Values[a]

		$E_{1/2}$ (V vs SCE)		
complex	pH	couple III	couple II	couple I
1	1	−0.78	−0.22	0.44
	3.3	−1.01	−0.46	0.31
	5.7	−1.20	−0.64	0.30
	7.2		−0.74	0.30
3	1	−0.83	−0.32[b]	0.44
	3.3	−1.02	−0.46	0.32
	5.7	−1.21	−0.60	0.31
	7.2			0.31
5	1	−0.71	−0.20	0.47
	3.3	−0.90	−0.46	0.37
	5.7		−0.63	0.36
	7.2		−0.75	0.36

[a]For measurement at pH 1: 0.1 M CF_3SO_3H as the electrolyte; glassy carbon was the working electrode, saturated calomel electrode (SCE) was the reference electrode, and platinum wire was the counter electrode. For measurement at pH 1.8−12: Britton−Robinson buffer as electrolyte; all other conditions the same as for pH 1.[39] [b]E_{pa} of the irreversible wave is reported. Couple II of **3** is irreversible at pH 1−2.21 but becomes reversible at pH 2.56−6.37. The reduction couples of **3** are ill-defined at pH >6.37.

of couple II is about twice that of couples I and III. As the pH increases from 1 to 3.3 (**1**, **3**) or 2.6 (**5**), the potentials for couples I−III shift cathodically with a slope of ca. 60 mV/pH, as depicted in Figure 7. Rotating disk electrode voltammetry of **1**·OTf, **3**·OTf, and **5**·OTf at pH 2 revealed that the coulombic stoichiometry in couples I−III has a ratio of 1:2:1 (Figures S18−S20 in the Supporting Information). At pH 1−3.3 (**1**, **3**) or 1−2.6 (**5**), couple I is reasonably attributed to the $Re^{VI/V}$ couple (eq 1). The $Re^{VI/V}$ potential is less anodic than that of *cis*-$[Re^{V}(O)_2(bpy)(py)_2]^+$ ($E_{1/2}$ = 0.62 V vs SCE at pH 2).[15b] Couple II is assigned as a two-electron reduction of Re(V) to Re(III) (eq 2), while couple III is attributable to the reduction of Re(III) to Re(II) (eq 3). The slope of 60 mV/pH is in accordance with one-electron one-proton reaction (eqs 1 and 3) and two-electron two-proton reaction (eq 2) according to the Nernst equation.[37,38]

At pH 1−3.3 (**1**) or pH 1−2.6 (**5**):

$$\text{couple I:}\quad \textit{cis}\text{-}[Re^{VI}(O)_2(L)]^{2+} + e^- + H^+ \rightarrow \textit{cis}\text{-}[Re^{V}(O)(OH)(L)]^{2+} \qquad (1)$$

$$\text{couple II:}\quad \textit{cis}\text{-}[Re^{V}(O)(OH)(L)]^{2+} + 2e^- + 2H^+ \rightarrow \textit{cis}\text{-}[Re^{III}(OH)(OH_2)(L)]^{2+} \qquad (2)$$

$$\text{couple III:}\quad \textit{cis}\text{-}[Re^{III}(OH)(OH_2)(L)]^{2+} + e^- + H^+ \rightarrow \textit{cis}\text{-}[Re^{II}(OH_2)_2(L)]^{2+} \qquad (3)$$

Upon further increasing the pH above 3.3 (**1**, **3**) or 2.6 (**5**), the potential of couple I becomes insensitive to pH change, indicative of a one-electron redox that does not involve proton transfer. At pH > 3.3 (**1**, **3**) or pH > 2.6 (**5**), the electrochemical reactions for the $Re^{VI/V}$, $Re^{V/III}$, and $Re^{III/II}$ couples are represented by eqs 4, 5, and 6, respectively. In the Pourbaix diagrams of **1**, **3**, and **5** (Figure 8), the breakpoint of

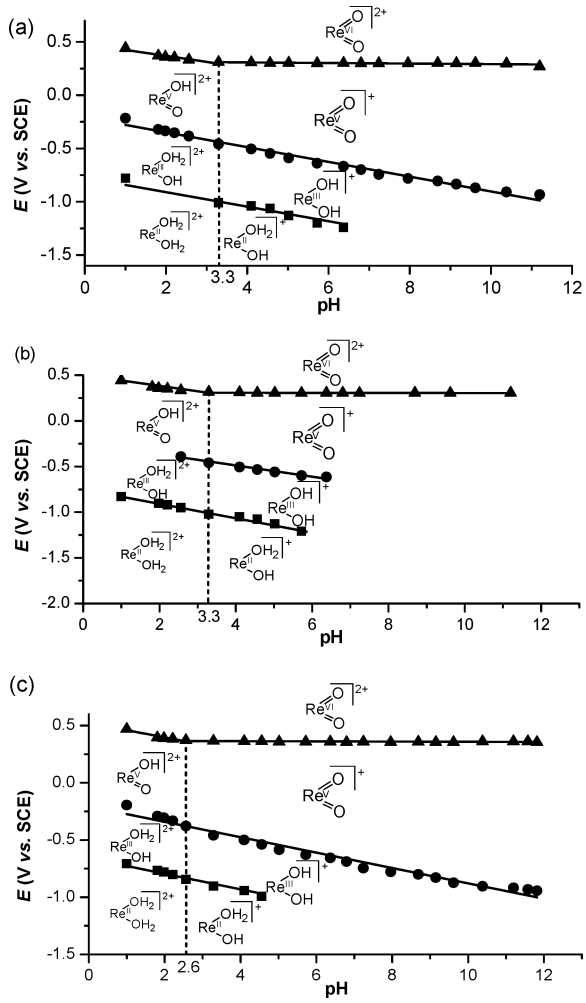

Figure 8. Pourbaix diagrams of (a) *cis*-$[Re^{V}(O)_2(pyxn)]$OTf (**1**·OTf), (b) *cis*-$[Re^{V}(O)_2(R,R\text{-pdp})]$OTf (**3**·OTf), and (c) *cis*-$[Re^{V}(O)_2(bqcn)]$OTf (**5**·OTf).

the plot of couple I is logically the pK_a value of *cis*-$[Re^{V}(O)_2(N_4)]^+$/*cis*-$[Re^{V}(OH)(O)(N_4)]^{2+}$ proton-transfer reaction, which was found to be 3.3, 3.3, and 2.6 for **1**, **3**, and **5**, respectively.

At pH >3.3 (**1**) or pH >2.6 (**5**):

$$\text{couple I:}\quad \textit{cis}\text{-}[Re^{VI}(O)_2(L)]^{2+} + e^- \rightarrow \textit{cis}\text{-}[Re^{V}(O)_2(L)]^{+} \qquad (4)$$

$$\text{couple II:}\quad \textit{cis}\text{-}[Re^{V}(O)_2(L)]^{+} + 2e^- + 2H^+ \rightarrow \textit{cis}\text{-}[Re^{III}(OH)_2(L)]^{+} \qquad (5)$$

$$\text{couple III:}\quad \textit{cis}\text{-}[Re^{III}(OH)_2(L)]^{+} + e^- + H^+ \rightarrow \textit{cis}\text{-}[Re^{II}(OH)(OH_2)(L)]^{+} \qquad (6)$$

DOI: 10.1021/acs.inorgchem.7b02404
Inorg. Chem. XXXX, XXX, XXX−XXX

Molecular Orbital Diagram. With reference to Vanquickenborne's work on *cis*-dihalogenotetraamine osmium(II) complexes,[40] the d orbitals of *cis*-dioxo metal complexes with C_{2v} symmetry are in the order of $d_{xz} < d_{yz} < d_{xy} < d_{z^2} < d_{x^2-y^2}$ (Figure 9).[41] In this work, the DFT-calculated molecular orbital

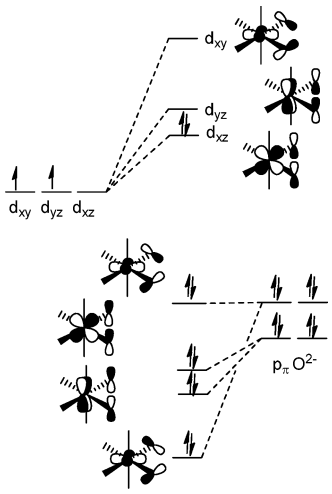

Figure 9. Molecular orbital diagram of *cis*-dioxo d^2 complex assuming a C_{2v} symmetry.[41]

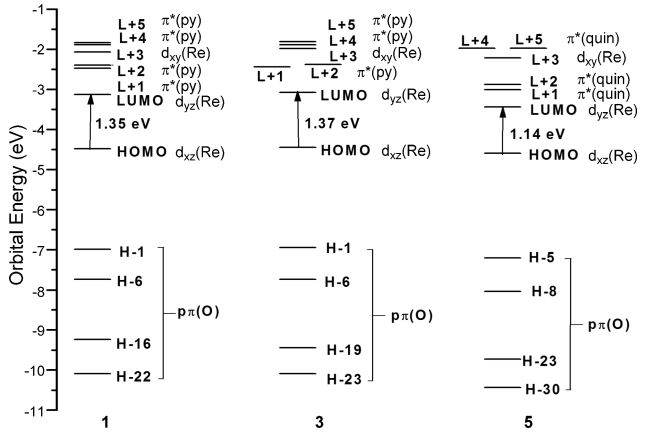

Figure 10. Molecular orbital diagrams of the *cis*-dioxorhenium(V) complexes **1**, **3**, and **5** at ground state (S_0).

diagrams for **1**, **3**, and **5** (Figure 10) at ground state show that the HOMO is mainly composed of the d_{xz} orbital while the LUMO and L+3 are mainly d_{yz}- and d_{xy}-based orbitals, respectively. The L+1 and L+2 are pyridyl/quinolyl-based orbitals.

The DFT-calculated molecular orbital diagram of *cis*-$[Re^{VI}(O)_2(pyxn)]^{2+}$ (**1′**) is shown in Figure 11. The singly occupied molecular orbital (SOMO) is mainly composed of d_{xz}(Re) orbital, supporting the assignment of a d^1 Re(VI) electronic configuration. The $d\pi^*$(Re) orbitals of **1′** (−6.5 to −3.7 eV) are at an energy lower than that of its Re(V) counterpart (**1**: −4.5 to −2 eV), in accordance with the higher electron affinity of Re(VI) relative to Re(V).

UV−Visible Absorption Spectra. The UV−vis absorption spectra of the *cis*-dioxorhenium(V) complexes are depicted in Figures 11 and 12, and the spectral data are given in Table 6.

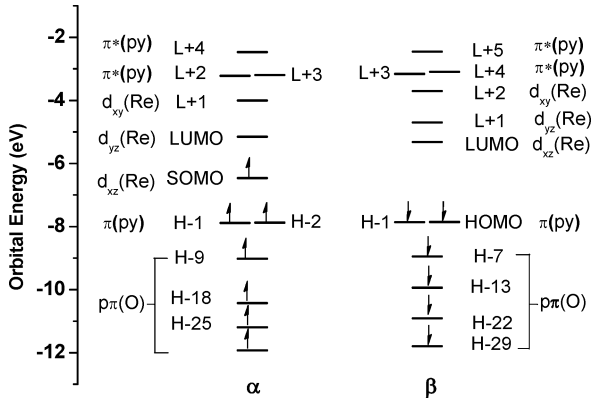

Figure 11. Molecular orbital diagram of *cis*-$[Re^{VI}(O)_2(pyxn)]^{2+}$ (**1′**) at doublet ground state.

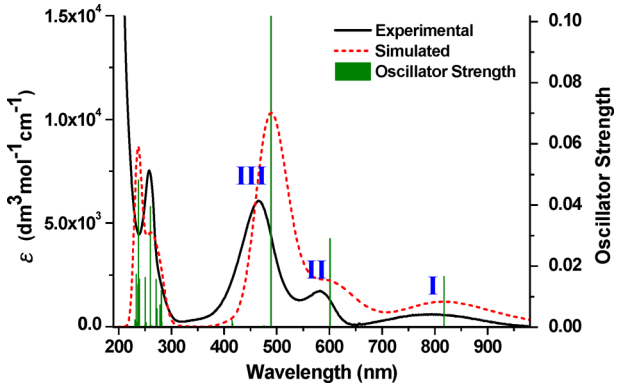

Figure 12. Experimental and simulated UV−vis absorption spectra of *cis*-$[Re^{V}(O)_2(pyxn)]^{+}$ (**1**) in acetonitrile solution.

Table 6. UV−Visible Absorption Data of *cis*-Dioxorhenium Complexes, $(1\cdot H^+\cdot OTf)_2$, and *trans*-2 in Acetonitrile Solution[a]

complex	λ_{abs} (nm) (ε (dm^3 mol^{-1} cm^{-1}))
1	800 (600), 580 (1740), 465 (6050), 345 (sh, 340), 258 (7380)
***cis*-2**	702 (450), 580 (700), 459 (4000), 270 (10250)
3	784 (700), 572 (2520), 462 (5570), 348 (200), 257 (7050)
4	688 (640), 564 (1300), 461 (4860), 268 (13470)
5	846 (1730), 591 (5580), 523 (sh, 3170), 384 (1080), 206 (10240), 297 (sh, 9420), 268 (6160)
1′	591 (77), 340 (2270), 296 (4580), 249 (10080)
1·H^+	238 (12200), 309 (5450), 900 (120)
***trans*-2**	449 (1010), 355 (1660), 310 (1600), 267 (9860)

[a]Measured in acetonitrile at 298 K.

The spectra of *cis*-$[Re^{V}(O)_2(pyxn)]PF_6$ (**1**·PF_6), *cis*-$[Re^{V}(O)_2(pyxn)]PF_6$ (***cis*-2**·PF_6), *cis*-$[Re^{V}(O)_2(R,R\text{-pdp})]PF_6$ (**3**·PF_6), and *cis*-$[Re^{V}(O)_2(R,R\text{-6-Me}_2\text{pdp})]BPh_4$ (**4**·BPh_4) in MeCN are similar but distinctively different from that of *cis*-$[Re^{V}(O)_2(bqcn)]PF_6$ (**5**·PF_6) (Table 6). Complexes **1**, ***cis*-2**, **3**, and **4** show three absorption bands at 688−800 nm (band I), ∼570 nm (band II). and ∼460 nm (band III). On the basis of the results of TDDFT calculations (Figure 12 and Figures S21−S23 and Table S16 in the Supporting Information), the weak absorption (band I) at ∼750 nm with an extinction coefficient of 450−700 dm^3 mol^{-1} cm^{-1} is derived from the HOMO → LUMO transition attributable to a $^1[d_{xz}(Re) \rightarrow d_{yz}(Re)]$ transition, which is at a slightly lower energy in

DOI: 10.1021/acs.inorgchem.7b02404
Inorg. Chem. XXXX, XXX, XXX−XXX

comparison to the assigned d−d transition of *cis*-$[Re^{V}(O)_2(OH_2)(Me_3tacn)]^+$ (~680 nm).[16] A similar low-energy absorption band at 750 nm (ε = 250 dm^3 mol^{-1} cm^{-1}) has also been observed in the electronic absorption spectrum of *cis*-$[Os^{VI}(O)_2(bpy)_2]^{2+}$.[12a] The absorption band at ~580 nm (band II) likely comes from a $^1[d_{xz}(Re) \rightarrow d_{xy}(Re)]$ transition mixed with $^1[d_{xz}(Re) \rightarrow \pi^*(L)]$ character. The intense absorption band at ~465 nm (band III) is mainly derived from the $^1[d_{xz}(Re) \rightarrow \pi^*(L)]$ transition, though TDDFT calculations show mixed character from a $^1[d_{xz}(Re) \rightarrow d_{xy}(Re)]$ transition. As a result, these two bands, mainly MLCT in nature, display relatively larger extinction coefficients of 700−2600 and 4000−6000 dm^3 mol^{-1} cm^{-1}, respectively. In addition, band I of ***cis*-2** and **4**, having 6-methyl substituents on the pyridyl group, are slightly blue shifted in comparison to those of **1** and **3**, respectively. This could be attributed to the larger O−Re−O angle (α) in ***cis*-2** and **4** (Table 3), which leads to LUMO destabilization, as reported in the work by Demanchy and Jean.[41,42] This is also consistent with calculations that the LUMOs of ***cis*-2** and **4** are at higher energy than those of **1** and **3** (**1**, −2.81 eV; ***cis*-2**, −2.58 eV; **3**, −2.77 eV; **4**, −2.53 eV).

The absorption spectrum of *cis*-$[Re^{V}(O)_2(bqcn)]PF_6$ (**5**·PF_6) in MeCN exhibits three absorption bands at around 846 nm (band I), 591 nm (band II), and 523 nm (band III) (Figure 13b). Band I can be correlated to the HOMO → LUMO transition attributable to $^1[d_{xz}(Re) \rightarrow d_{yz}(Re)]$, though with a larger ε value (1730 dm^3 mol^{-1} cm^{-1}) in comparison to those of **1**, ***cis*-2**, **3**, and **4**. Band II at 591 nm (ε = 5580 dm^3 mol^{-1} cm^{-1}) is derived from the HOMO → L+2 transition attributable to a $^1[d_{xz}(Re) \rightarrow \pi^*(quinolyl)]$ transition. Band III at 523 nm (ε = 3170 dm^3 mol^{-1} cm^{-1}) can be assigned to $^1[d_{xz}(Re) \rightarrow d_{xy}(Re)]$ (HOMO → L+3), mixed with a $^1[d_{xz}(Re) \rightarrow \pi^*(quinolyl)]$ transition.

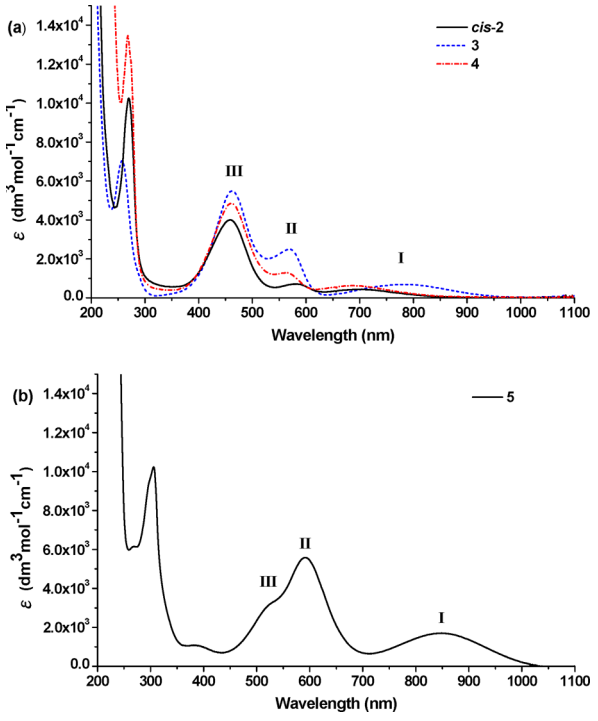

Figure 13. Experimental UV−vis absorption spectra of *cis*-dioxorhenium(V) complexes (a) ***cis*-2**·PF_6, **3**·PF_6, and **4**·BPh_4 and (b) **5**·PF_6 in acetonitrile solution.

The UV−vis absorption spectrum of *cis*-$[Re^{VI}(O)_2(pyxn)](PF_6)_2$ (**1′**·$(PF_6)_2$) displays three absorption bands in the UV spectral region at 340, 296, and 249 nm (ε = 2270, 4580, and 10080 dm^3 mol^{-1} cm^{-1}, respectively) and a weak absorption band at 591 nm (ε = 77 dm^3 mol^{-1} cm^{-1}) (Figure 14). For this complex, the lowest-energy transition is derived from the SOMO → LUMOα transition attributable to $^2[d_{xz}(Re) \rightarrow d_{xy}(Re)]$.

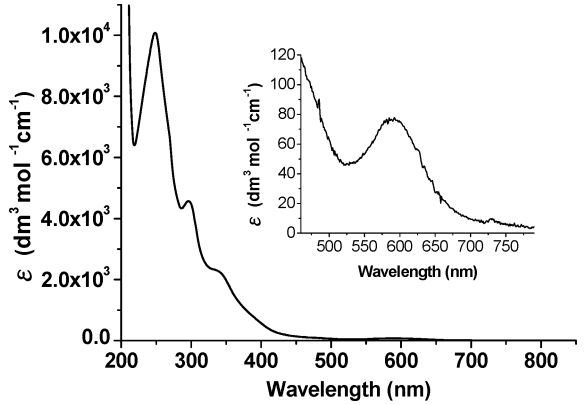

Figure 14. Experimental UV−vis absorption spectrum of *cis*-$[Re^{VI}(O)_2(pyxn)](PF_6)_2$ (**1′**·$(PF_6)_2$) in acetonitrile solution.

For *cis*-$[Re^{V}(O)(OH)(pyxn)]^{2+}$ (**1**·H^+), its UV−vis absorption spectrum in the visible spectral region is featureless (Figure 15). Intense absorption bands are located in the UV spectral region at 309 and 238 nm (ε = 5450 and 12200 dm^3 mol^{-1} cm^{-1}, respectively). The weak absorption band at ~900 nm (ε = 120 dm^3 mol^{-1} cm^{-1}) is assignable to a $^1[d_{xz}(Re) \rightarrow d_{yz}(Re)]$ transition. The high-energy absorption bands are attributable to a mixture of MLCT and LMCT transitions such as $^1[d\pi(Re) \rightarrow \pi^*(py)]$ and $^1[p\pi(O) \rightarrow d\pi(Re)]$.

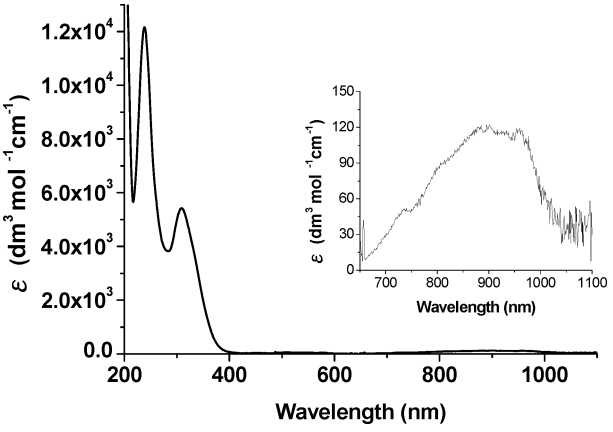

Figure 15. Experimental UV−vis absorption spectrum of *cis*-$[Re^{V}(O)(OH)(pyxn)](OTf)_2$ (**1**·H^+·$(OTf)_2$) in acetonitrile solution.

The electronic absorption spectrum of *trans*-$[Re^{V}(O)_2(6\text{-}Me_2pyxn)]PF_6$ (***trans*-2**·PF_6) displays two broad absorption bands at 449 and 355 nm with ε = 1010 and 1660 dm^3 mol^{-1} cm^{-1}, respectively (Figure 16). The low-energy band at 449 nm is derived from the HOMO → LUMO transition attributable to a $^1[d_{xy}(Re) \rightarrow \pi^*(py)]$ MLCT transition. The high-energy

DOI: 10.1021/acs.inorgchem.7b02404
Inorg. Chem. XXXX, XXX, XXX−XXX

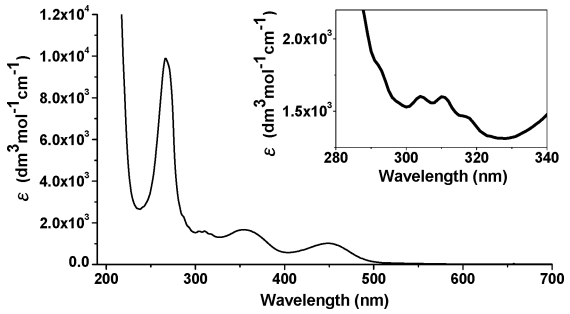

Figure 16. Experimental UV−vis absorption spectrum of *trans*-$[Re^{V}(O)_2(6\text{-}Me_2pyxn)]PF_6$ (***trans*-2**·PF_6) in acetonitrile solution (inset: expanded region at 280−340 nm).

band at 355 nm is mainly composed of a $^1[d_{xy}(Re) \rightarrow \pi^*(py)]$ transition, mixed with $^1[d_{xy}(Re) \rightarrow \pi^*(d(Re)\text{-}p(O))]$ transition. The vibronic band at 310 nm is attributed to a $^1[p\pi(O) \rightarrow \pi^*(d\pi(Re)\text{-}p(O))]$ LMCT transition. The progressional spacing of ca. 684 cm^{-1} corresponds to the weakened Re−O bond in the excited state in comparison to the ground state $\nu_{asym}(ReO_2)$ stretch (785 cm^{-1}) in the IR spectrum. The intense absorption band at 267 nm is mainly composed of transitions involving electron promotion from the H-4/H-5 orbital to LUMO/L+1 orbital, which are assigned to $^1[\pi(py) \rightarrow \pi^*(d(Re)\text{-}p(O))]$ transitions.

Reactivity. The oxygen-atom transfer reactivity of the *cis*-$[Re^{V}(O)_2]^+$ complexes was evaluated from the reaction of **1**·PF_6 with triphenylphosphine, thioanisole, and styrene. In acetonitrile under aerobic conditions, **1** was not able to oxidize the tested substrates even at elevated temperatures (up to 60 °C) for 4 h. No oxidation product such as phosphine oxide, sulfoxide, or epoxide could be detected by GC-MS. UV−vis absorption measurements of the reaction mixtures revealed that **1** remained intact.

cis-$[Re^{V}(O)_2(pyxn)]^+$ (**1**; 0.1 mM) reacts with excess Lewis acids (10 mM) including Sc^{3+}, Zn^{2+}, Li^+, and CF_3SO_3H in acetonitrile to give a pink solution. UV−vis spectroscopy showed that a common species that absorbed at 238 and 308 nm was produced, irrespective of the choice of Lewis acids. ESI-MS measurement of the pink solution revealed the formation of doubly charged species at *m*/*z* 272.11, assignable to the protonated form of **1**, *cis*-$[Re^{V}(O)(OH)(pyxn)]^{2+}$ (**1**·H^+). Complex **1**·H^+ has been crystallographically characterized (vide supra, Figure S9 in the Supporting Information).

The formation of **1**·H^+ from the reaction of **1** with $Sc^{III}(OTf)_3$ was followed by UV−vis titration, featuring an isosbestic point at 370 nm (Figure S27 in the Supporting Information). Only 0.5 equiv of $Sc^{III}(OTf)_3$ was sufficient to quantitatively protonate **1** (the proton likely comes from reaction of $Sc^{III}(OTf)_3$ with a trace amount of water in the solvent). When CF_3SO_3H was used as the titrant, 1.0 equiv was required for complete reaction (Figure 17). The reaction was reversible; **1**·H^+ could be converted back to **1** by addition of 1.0 equiv of triethylamine. When weaker Lewis acids such as $Zn(OTf)_2$ and LiOTf were used as titrants, the reaction was not complete at a low titrant concentration (e.g., up to 20 equiv), suggesting that a binding equilibrium exists.

In aqueous solutions, **1**·OTf exhibits pH-dependent absorption profiles in the range of pH 1.8−4.8 (Figure 18).

cis-$[Re^{VI}(O)_2(pyxn)]^{2+}$ (**1′**) is thermally stable; insignificant decomposition was observed by heating its acetonitrile solution at 80 °C for 18 h. However, **1′** is sensitive to aliphatic amines.

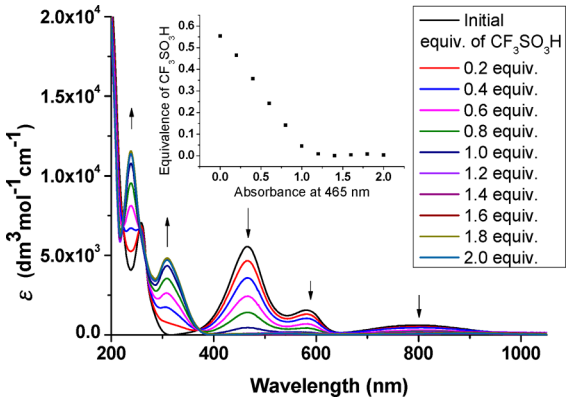

Figure 17. UV−vis titration of an acetonitrile solution of **1**·PF_6 (0.1 mM) with CF_3SO_3H.

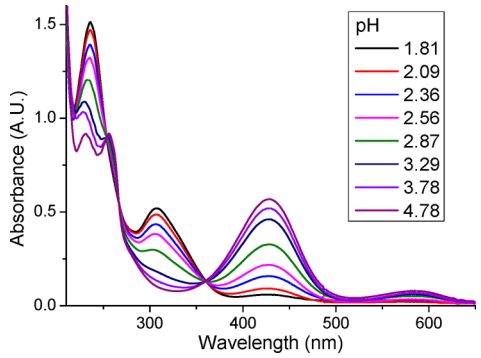

Figure 18. Experimental UV−vis absorption spectrum of *cis*-$[Re^{V}(O)_2(pyxn)]OTf$ (**1**·OTf; 1×10^{-4} M) in aqueous solution at different pHs (Britton−Robinson buffer).[39]

For example, in acetonitrile, **1′** was observed to be reduced back to **1** (>80% by using UV−vis spectroscopy) in the presence of a few equivalents of triethylamine or triethanolamine. Another *cis*-dioxorhenium(VI) complex, [(Tp)-$Re^{VI}(O)_2(Cl)$], has also been mentioned to be decomposed by bases.[22]

Interestingly, **1′** was found to oxidize hydrocarbons with weak C−H bonds (bond dissociation energy (BDE): 75.5−76.3 kcal mol^{-1}) stoichiometrically (Table 7). For instance, reaction of **1′** (1.0 equiv) with 1,4-cyclohexadiene (CHD) in acetonitrile at 80 °C for 1 h afforded benzene (0.485 equiv) as an aromatization product. The product yield based on Re was 97%, considering a reaction stoichiometry of Re:CHD = 2:1. The reaction was accompanied by a color change from green to purple-pink. UV−vis measurement of the resultant solution showed absorption bands at 238 and 308 nm characteristic of **1**·H^+. Upon treatment with triethylamine, **1** was quantitatively produced (quantified at 465 nm) on the basis of the initial concentration of **1′**. In a control experiment where **1′** was replaced by **1**, no benzene could be detected after 3 h at 80 °C.

Complex **1′** similarly reacted with 9,0-dihydroanthracene (9,10-DHA) to give anthracene in 98% yield. A competitive reaction between 9,10-DHA and 9,10-DHA-d_4 suggested a primary kinetic isotope effect (KIE) of $k_H/k_D = 4.9$. Reaction of **1′** with xanthene gave xanthone in 90% yield ($k_H/k_D = 5.8$). Under identical conditions, no substrate conversion was noticed in the reaction of **1′** with fluorene, tetralin, or styrene.

DOI: 10.1021/acs.inorgchem.7b02404
Inorg. Chem. XXXX, XXX, XXX−XXX

Table 7. Stoichiometric Oxidation of Hydrocarbons by *cis*-$[Re^{VI}(O)_2(pyxn)](PF_6)_2$ (1′·$(PF_6)_2$) in Acetonitrile at 80 °C

substrate	BDE (kcal mol^{-1}) [a]	reaction time (h)	product	yield (%) [b]
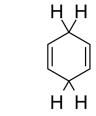	76	1		97
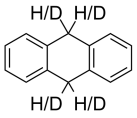	76.3	1.5	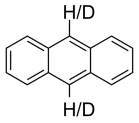	98 (KIE = 4.9)
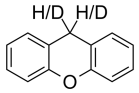	75.5	2	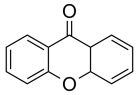	90 (KIE = 5.8)

[a]Values adopted from ref 52. [b]Product yield calculated on the basis of 1′ acting as a one-electron oxidant and oxidation of CHD to benzene as a two-electron process, 9,10-DHA to anthracene as a two-electron process, and xanthene to xanthone as a four-electron process.

DISCUSSION

There have been extensive works on *trans*-dioxo d^2 metal complexes,[1,2b,i,j,3−10] whereas their *cis*-dioxo counterparts have been comparatively less explored, with the octahedral species having a few well-characterized examples.[11−17] Interesting types of *cis*-dioxo d^2 metal complexes to be developed are the octahedral species bearing chiral tetradentate ligands currently employed in asymmetric oxidation reactions, such as the neutral C_2-symmetric N_4 ligands pyxn, pdp, and bqcn and their derivatives, which have been increasingly used in iron and manganese catalysis.[29−31] We have endeavored to try to explore a synthetic route to chiral d^2 *cis*-$[M(O)_2(N_4)]^{n+}$ (M = Fe, Mn) species; such attempts, however, have not been successful. In the literature, there have been a lack of isolated examples for *cis*-$Fe^{VI}O_2$ and *cis*-$Mn^{V}O_2$ complexes, owing to their high reactivity/instability. Nam and co-workers reported the generation of the monooxo d^3 manganese(IV) complex $[Mn^{IV}(O)(OH_2)(bqcn)]^{2+}$ from $[Mn^{II}(OTf)_2(bqcn)]$ by oxidation with cerium(IV) ammonium nitrate in the presence of water;[43a] this monooxo complex can also be generated by oxidation with $[Ru^{III}(bpy)_3]^{3+}$ in aqueous solution or by photocatalytic generation with water as an oxygen source, as reported by Nam and Sun.[43b] In view of the evidence, provided by ESI-MS analysis, for the formation of *cis*-$[Mn^{V}(O)_2(S,S\text{-bqcn})]^{+}$ intermediate in the reaction of $[Mn^{II}(Cl)_2(S,S\text{-bqcn})]$ with Oxone[31b] and the periodic relationship between Mn and Re, together with the fact that high-valent Re-oxo complexes are relatively nonoxidizing and more stable, Re was the metal of choice in this work for the generation of relatively stable *cis*-dioxo metal complexes having d^2 (and also d^1) electronic configurations supported by tetradentate N_4 ligands.

Note that, in addition to *cis*-$[Mn^{V}(O)_2(S,S\text{-bqcn})]^{+}$ bearing the C_2-symmetric N_4 ligand bqcn, a *cis*-$[M(O)_2(N_4)]^{n+}$ intermediate with another type of neutral N_4 ligand, *N*,*N*′-dimethyl-2,11-diaza[3.3](2,6)pyridinophane (L-N_4Me_4), i.e. *cis*-$[Fe^{V}(O)_2(L\text{-}N_4Me_4)]^{+}$, was previously proposed, with support by ESI-MS analysis and DFT calculations, in *cis*-$[Fe^{III}(Cl)_2(N_4)]^{+}$-catalyzed *cis*-dihydroxylation of alkenes with Oxone.[44] This *cis*-$Fe^{V}(O)_2$ species was also highly reactive and has not been isolated.

Despite the reports of a number of isolated and structurally characterized d^2 *cis*-dioxorhenium(V) complexes, the majority of these are five-coordinate complexes adopting a trigonal-bipyramidal configuration,[23−27] with three examples of structurally characterized octahedral ones.[15−17] The complex *cis*-$[Re^{V}(O)_2(cyclen)]^{+}$, bearing an achiral N_4 ligand and formulated by ^{1}H NMR analysis, was not isolated in pure form.[28] To the best of our knowledge, structurally characterized (by X-ray crystallography) examples of *cis*-$Re^{V}O_2$ supported by a tetradentate ligand have not been reported in the literature, nor have d^2 *cis*-$[M(O)_2(N_4)]^{n+}$ complexes (N_4 = pyxn, pdp, bqcn, and their derivatives) been isolated.

In this work, the new class of *cis*-dioxorhenium(V) complexes *cis*-$[Re^{V}(O)_2(N_4)]^{+}$ supported by different neutral N_4 ligands (pyxn, *R*,*R*-pdp, bqcn, 6-Me_2pyxn, *R*,*R*-6-Me_2pdp) and *trans*-$[Re^{V}(O)_2(6,6'\text{-}Me_2pyxn)]PF_6$ were synthesized. All complexes (**1**, ***cis*-2**, **3**−**5**, ***trans*-2**, **1**′) have been structurally characterized by X-ray crystallography. The coordination geometry is affected by the ligand structure. For complexes bearing an N_4 ligand with a rigid bipyrrolidyl backbone (*R*,*R*-pdp in **3** and *R*,*R*-6-Me_2pdp in **4**) and those bearing a cyclohexyl backbone without *o*-methyl substitution (pyxn in **1** and bqcn in **5**), the cis-α isomer was exclusively obtained, consistent with the cis coordination mode adopted by such N_4 ligands in their octahedral Fe and Mn complexes.[29−31] However, for **2** bearing an N_4 ligand with a cyclohexyl backbone and with *o*-methyl aromatic substitution (6-Me_2pyxn), both cis-α and trans isomers were obtained. In the preparation of **2**, the trans isomer was isolated as the major product after purification. This could be associated with the relatively high flexibility of the cyclohexyl backbone[45] (coupled with the steric effect of the 6-Me substituents on the pyridyl groups), which allowed the ligand to adopt multiple coordination modes to the Re(V) center. ***trans*-2** was found to isomerize into a mixture of ***trans*-2** and ***cis*-2** under thermal conditions. At equilibrium, the cis/trans ratio was ∼2.1 (at 50 °C). The kinetics and thermodynamics of the isomerization have been determined, showing an activation barrier ($\Delta G^{\ddagger}$) of 102.7−104.7 kJ mol^{-1} and a small free energy difference ($\Delta\Delta G^{\ddagger}$) of 2.0 kJ mol^{-1} between the two isomers. The fact that the cis isomer is slightly more stable is quite surprising for a d^2-$M(O)_2$ system, because the electronic repulsion between the two oxo ligands can be relaxed in the trans configuration. Perhaps, in the trans geometry of **2**, the highly strained bonding angles greatly destabilize the molecules and outweigh the effect of the electronic repulsion.

The isolation of ***trans*-2** bearing the 6-Me_2pyxn ligand is rather unusual. Previously, several examples of structurally characterized octahedral metal complexes with this ligand have been reported, including $[Fe^{II}(Hdbc)(6\text{-}Me_2pyxn)]OTf$ (Hdbc = 3,5-di-*tert*-butyl-1,2-catecholate monoanion),[46a] $[Fe^{III}(dbc)(6\text{-}Me_2pyxn)]OTf$,[46a] $[Fe^{II}(OTf)_2(6\text{-}Me_2pyxn)]$,[29a] $[Fe^{II}(H(4\text{-nc}))(6\text{-}Me_2pyxn)]OTf$ (H_2(4-nc) = 4-nitrocatechol),[46b] and $[Mn^{II}(H(4\text{-nc}))(6\text{-}Me_2pyxn)]OTf$,[46b] which all adopt a cis configuration. In addition, the cis configuration observed for these Fe and Mn complexes of 6-Me_2pyxn exclusively belongs to cis-β, in contrast to the cis-α configuration found for ***cis*-2** in this work. Thus, the d^2 *cis*-$Re^{V}(O)_2$ unit appears to have a significant effect on the coordination mode of the 6-Me_2pyxn ligand.

Complexes ***trans*-2** and ***cis*-2** bearing the same ligand contribute a unique pair of structurally characterized trans and cis isomers of d^2 $Re^{V}(O)_2$ complexes. In previously

DOI: 10.1021/acs.inorgchem.7b02404
Inorg. Chem. XXXX, XXX, XXX−XXX

reported *cis*-$Re^{V}(O)_2$ complexes,[15−17,23−27] the ligands employed are different from those in the *trans*-$Re^{V}(O)_2$ complexes.[3,4,5a,b,6c,7g,8−10] For example, *trans*-$[Re^{V}(py)_4(O)_2]^{+}$ [3] bears monodentate pyridine ligands, whereas a bidentate bpy ligand was used for isolation of the corresponding cis analogue (*cis*-$[Re^{V}(O)_2(bpy)(py)_2]^{+}$).[15]

Electrochemical studies revealed some interesting properties of the *cis*-dioxorhenium(V) complexes. In nonaqueous medium (acetonitrile), complexes **1**, ***cis*-2**, and **3**−**5** all show a $Re^{VI/V}$ oxidation couple at relatively low potentials (0.39−0.49 V vs SCE), being ca. 0.3 V less than that for the oxidation of *cis*-$[Re^{V}(O)_2(bpy)(py)_2]^{+}$ (0.77 V vs SCE).[15c] In comparison to the latter complex, the greater stabilization of the Re^{VI} oxidation state in the *cis*-$[Re^{VI}(O)_2(N_4)]^{2+}$ complexes is ascribed to the stronger σ-donor strength of tertiary amine N-donor atoms. Meyer and co-workers previously showed that *cis*-$[M^{VI}(O)_2(bpy)_2]^{2+}$ (M = Ru, Os) complexes are accessible through successive proton-coupled electron transfer (PCET) reactions of *cis*-$[M^{II}(OH_2)_2(bpy)_2]^{2+}$.[18a] For **1**, **3**, and **5**, in aqueous media, three PCET reactions corresponding to $Re^{VI/V}$, $Re^{V/III}$, and $Re^{III/II}$ couples are observed at pH 1 over a potential range of ca. 1.2 V. The pK_a values of *cis*-$[Re^{V}(O)_2(N_4)]^{+}$/*cis*-$[Re^{V}(OH)(O)(N_4)]^{2+}$ (3.3 for **1** and **3**, 2.6 for **5**) are higher than that of *cis*-$[Re^{V}(O)_2(bpy)(py)_2]^{+}$/*cis*-$[Re^{V}(OH)(O)(bpy)(py)_2]^{2+}$ (pK_a < 1, based on the Pourbaix diagram showing $Re^{VI/V}$ potential independent of pH in the range of 1−11,[15b] i.e. protonation of *cis*-$[Re^{V}(O)_2(bpy)(py)_2]^{+}$ to give *cis*-$[Re^{V}(O)(OH)(bpy)(py)_2]^{2+}$ was not observed over this pH range), which is attributable to stronger σ donation of N_{amine} in comparison to that of N_{py}. The present finding shows that the oxo ligands of **1**, **3**, and **5** are more basic in comparison with those of *cis*-$[Re^{V}(O)_2(bpy)(py)_2]^{+}$. For an additional comparison, the pK_a value of the *trans*-$[Re^{V}(O)_2(4\text{-}NMe_2py)_4]^{+}$/*trans*-$[Re^{V}(OH)(O)(4\text{-}NMe_2py)_4]^{2+}$ proton-transfer reaction was determined to be 2.3 by a spectrophotometric titration method.[15c] The basicity of the oxo ligands is reflected in the reaction of **1** with Lewis acids. Upon treatment of a stoichiometric amount of a strong Lewis acid such as Sc^{III} or a protic acid such as CF_3SO_3H, **1** is readily protonated to give *cis*-$[Re^{V}(O)(OH)(pyxn)]^{2+}$ (**1**·H^{+}), which has been isolated and structurally characterized.

The ease of protonation of **1** in both nonaqueous and aqueous media gives rise to interesting spectroscopic observations of the acid−base pair. Even though there is only a slight difference in the Re−O distances of **1** (1.750(5) and 1.753(5) Å) and **1**·H^{+} (1.788(5) Å), tremendous differences exist in both the UV−vis absorption spectra and the electrochemistry. Upon protonation, the MLCT transition band of **1** substantially blue-shifts from 465−580 to 309 nm in acetonitrile (Figure 17) or from 429−584 to 307 nm in aqueous solutions (Figure 18), suggesting significant stabilization of the dπ(Re)-based orbitals as a result of breaking one π(Re−O) bond (Figure 8); the extent of the blue shift is even comparable to that resulting from one-electron oxidation of **1** to **1**′. In accordance with this, the cyclic voltammogram of **1**·H^{+} in acetonitrile shows a reversible Re(V)/Re(IV) couple at −0.31 V vs SCE (Figure 7), which is otherwise not observed for **1**. In addition, the Re(VI)/Re(V) oxidation potential shifted anodically by more than 0.5 V. Such features are unprecedented for *cis*-dioxorhenium(V) complexes.[15−17] As depicted in Figure 18, **1**·OTf exhibits reversible pH-dependent absorption profiles, with varying relative intensities of the absorption bands at 429 nm (for **1**) and 307 nm (for **1**·H^{+}) at moderately acidic pH values. The sensitivity of the MLCT transition energy and reversibility of the spectral changes of *cis*-dioxorhenium(V) with pH suggest that the latter may be used as a colorometric pH sensor.

The $Re^{VI/V}$ potentials and basicity of the Re(V) complexes (in aqueous medium) are valuable information, as they allow access to the hydrogen-atom affinity of *cis*-$[Re^{VI}(O)_2(N_4)]^{2+}$ complexes. According to the thermochemical method developed by Mayer and Bordwell (eq 7),[47] the bond dissociation energies (D_{O-H}) of *cis*-$[Re^{V}(O)(O-H)(L)]^{2+}$ to form *cis*-$[Re^{VI}(O)_2(L)]^{2+}$ (L = pyxn, PDP, bqcn) are calculated to be 74.5 (**1** and **3**, Scheme 1) and 75.1 kcal mol^{-1} (**5**). From these,

Scheme 1. Thermochemical Cycle of *cis*-$[Re^{VI}(O)_2(pyxn)]^{2+}$ (1′)

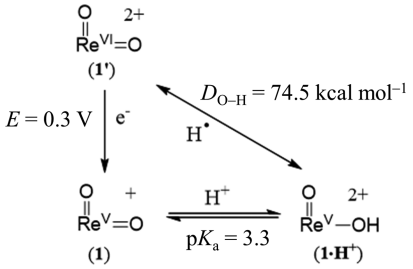

the *cis*-$[Re^{VI}(O)_2(N_4)]^{2+}$ complexes are estimated to be mild hydrogen-atom abstractors with slightly smaller D_{O-H} values in comparison to permanganate ($Mn^{VII}O_4^{-}$; 80 kcal mol^{-1}).[48]

$$D_{O-H} = 23.06E + 1.37pK_a + C \quad (7)$$

In accordance with the calculated hydrogen-atom affinity, *cis*-$[Re^{VI}(O)_2(pyxn)]^{2+}$ (**1**′) was found to stoichiometrically oxidize hydrocarbons with weak C−H bonds (BDE: 75.5−76.3 kcal mol^{-1}, three examples). A primary kinetic isotope effect (KIE) of 4.9−5.8 in intermolecular competitions is indicative of hydrogen atom abstraction at the rate-determining step or product-determining step.[49] Notably, substrates with C−H bond dissociation energies of >80 kcal mol^{-1} (e.g., fluorene, 82 kcal mol^{-1}; tetralin, 82.9 kcal mol^{-1}) could not be oxidized effectively.

Relative to *trans*-dioxo d^2 complexes,[1,2b,i,j,3−10] there have been limited reports on the electronic spectroscopy of *cis*-dioxo d^2 complexes. Theoretically, there are two singlet transitions within the Re(5dπ) orbitals for *cis*-dioxo d^2 metal complexes having C_{2v} symmetry, which are $^1[d_{xz}(Re) \rightarrow d_{yz}(Re)]$ and $^1[d_{xz}(Re) \rightarrow d_{xy}(Re)]$, respectively. On the other hand, there is only one $^1[d_{xy}(Re) \rightarrow \pi^*(d(Re)\text{-}p(O))]$ transition for *trans*-dioxo d^2 metal complexes with D_{4h} symmetry. According to the conventional molecular orbital diagrams for C_{2v} and D_{4h} systems,[50] the d−d splitting is expected to be smaller in *cis*-dioxo metal complexes than in *trans*-dioxo metal complexes. In the UV−vis absorption spectra of *cis*-$[Re^{V}(O)_2(N_4)]^{+}$ complexes, the $^1[d_{xz}(Re) \rightarrow d_{yz}(Re)]$ transition can be assigned to the absorption band at 680−850 nm with ε values of 450−1730 dm^3 mol^{-1} cm^{-1}, while the $^1[d_{xz}(Re) \rightarrow d_{xy}(Re)]$ transition contributes to the two absorption bands at 400−700 nm with ε values of 700−6050 dm^3 mol^{-1} cm^{-1}, the latter have substantial $^1[d_{xz}(Re) \rightarrow \pi^*(L)]$ character. In the case of ***trans*-2**, the $^1[d_{xy}(Re) \rightarrow \pi^*(d(Re)\text{-}p(O))]$ transition is mixed with a $^1[d_{xy}(Re) \rightarrow \pi^*(py)]$ MLCT transition (355 nm, ε = 1660 dm^3 mol^{-1} cm^{-1}). These mixed ligand-field and MLCT transitions are not suitable for direct comparison. Therefore, only the

DOI: 10.1021/acs.inorgchem.7b02404
Inorg. Chem. XXXX, XXX, XXX−XXX

wavelengths of the $^1[d_{xz}(Re) \rightarrow d_{yz}(Re)]$ transition of *cis*-$[Re^V(O)_2(N_4)]^+$ are used to compare with that of the $^1[d_{xy}(Re) \rightarrow \pi^*(d(Re)\text{-}p(O))]$ transition for *trans*-$[Re^V(O)_2(py)_4]^+$, *trans*-$[Re^V(O)_2(en)_2]^+$, and *trans*-$[Re^V(O)_2(CN)_4]^{3-}$ (350−600 nm; ε = 50−1200 $dm^3\ mol^{-1}cm^{-1}$);[4b] this matches with the hypothesis that the lowest-energy d−d transition in *cis*-dioxo d^2 metal complexes is smaller than that in *trans*-dioxo counterparts. In addition, the $^1[p\pi(O) \rightarrow d\pi^*(Re)]$ LMCT absorption band at 250−400 nm of *trans*-dioxorhenium(V) complexes shows characteristic vibronic structure with vibrational progressions of 600−800 cm^{-1} corresponding to excited state ν_{asym}(O−Re−O) stretches.[4b] On the basis of TDDFT results, the calculated LMCT $^1[p\pi(O) \rightarrow \pi^*(d\pi(Re)\text{-}p(O))]$ transitions of *cis*-$[Re^V(O)_2(N_4)]^+$ complexes are at ca. 240−280 nm but are difficult to observe in the experimental electronic absorption spectra due to the presence of intense ligand-centered absorption bands of the N_4 ligand at similar energies.

Structural and UV−vis absorption spectral data of *cis*-dioxo d^1 metal complexes[19−22] are also sparse in the literature. The *cis*-dioxo d^1 complex **1′** and its *cis*-dioxo d^2 counterpart **1** bear the same tetradentate pyxn ligand, and both adopt a pseudo-octahedral geometry. Isolation of the *cis*-$Re^{VI}(O)_2$ complex **1′** was realized by electrochemical oxidation of the *cis*-$Re^V(O)_2$ complex **1**. Previously, Mayer and co-workers prepared *cis*-$[(Tp)Re^{VI}(O)_2(X)]$ (X = Cl^-, Br^-, I^-), the only prior examples of octahedral d^1 *cis*-dioxo Re(VI), by chemical oxidation of the monooxo complexes $[(Tp)Re^V(O)(X)(OTf)]$ with pyridine *N*-oxide.[22] The crystal structure of **1′**, in comparison to that of **1**, reveals shorter Re−O distances and a smaller O−Re−O angle attributable to removal of one electron from the antibonding molecular orbital of d_{xz}(Re) and $p\pi$(O). Such an observation is in line with the slightly increased calculated Re−O bond orders of 2.2963 and 2.2956 based on NBO analyses of **1′** (Table S18 in the Supporting Information) relative to those of 2.2508 and 2.2505 for **1** (Table S17 in the Supporting Information). In contrast, the Re−O distances of *trans*-$[Re(O)_2(dmap)_4]^{n+}$ (dmap = 4-(dimethylamino)pyridine) are virtually the same in both the Re^V and Re^{VI} oxidation states (*n* = 1 and 2, respectively), as the HOMO d_{xy} orbital is nonbonding in *trans*-dioxo d^2 complexes with D_{4h} symmetry.[51] In the UV−vis absorption spectrum of **1′** (Re^{VI}), in comparison to that of **1** (Re^V), the MLCT $[d_{xz}(Re) \rightarrow \pi^*(py)]$ transition bands significantly blue shift to λ_{abs} <400 nm. This finding suggests that the $d\pi$(Re) orbitals of **1′** are at lower energies in comparison to those of **1**, resulting from the stronger electron affinity of the Re(VI) ion. Similarly, the d−d transition band also blue-shifts from 800 nm (for **1**) to 591 nm (for **1′**), indicating a larger d−d splitting that arises from the oxidation of Re(V) to Re(VI).

CONCLUSIONS

We have synthesized and characterized a number of *cis*-$[Re^V(O)_2(N_4)]^+$ complexes (N_4 = chiral tetradentate N_4 ligands including pyxn, 6-Me_2pyxn, *R,R*-pdp, *R,R*-6-Me_2pdp, and bqcn), together with *trans*-$[Re^V(O)_2(6\text{-}Me_2pyxn)]^+$ (an octahedral metal 6-Me_2pyxn complex which unusually adopts a trans configuration) and a sparse example of *cis*-$[Re^{VI}(O)_2(pyxn)]^{2+}$. Their structures were established by X-ray crystallography. The cyclic voltammograms of *cis*-dioxorhenium(V) complexes in MeCN (0.1 M $[NBu_4]PF_6$) and in 0.1 M CF_3SO_3H (pH 1) and the Pourbaix diagrams of *cis*-$[Re^V(O)_2(N_4)]OTf$ (N_4 = pyxn, *R,R*-pdp, bqcn) are presented. TDDFT calculations were performed to shed light on the experimentally observed electronic absorption properties of the *cis*-dioxorhenium(V) complexes and *cis*-$[Re^{VI}(O)_2(pyxn)]^{2+}$.

ASSOCIATED CONTENT

Supporting Information

The Supporting Information is available free of charge on the ACS Publications website at DOI: 10.1021/acs.inorgchem.7b02404.

Experimental procedures, characterization data, computational details and results, Figures S1−S27, and Tables S1−S42 (PDF)

Accession Codes

CCDC 1524881, 1551929−1551934, and 1560139 contain the supplementary crystallographic data for this paper. These data can be obtained free of charge via www.ccdc.cam.ac.uk/data_request/cif, or by emailing data_request@ccdc.cam.ac.uk, or by contacting The Cambridge Crystallographic Data Centre, 12 Union Road, Cambridge CB2 1EZ, UK; fax: +44 1223 336033.

AUTHOR INFORMATION

Corresponding Author

*E-mail for C.-M.C.: cmche@hku.hk.

ORCID

Xiaoyong Chang: 0000-0003-1394-6164
Jie-Sheng Huang: 0000-0003-1724-4362
Chi-Ming Che: 0000-0002-2554-7219

Author Contributions

‖V.Y.-M.N. and C.-W.T. contributed equally.

Notes

The authors declare no competing financial interest.

ACKNOWLEDGMENTS

This work was supported by the Hong Kong Research Grants Council (HKU 700813, 17303815), the National Key Basic Research Program of China (No. 2013CB834802), and the Basic Research Program of Shenzhen (No. JCYJ20160229123546997). This research was conducted in part using the research computing facilities and/or advisory services offered by Information Technology Services, The University of Hong Kong, and the HKU ITS research computing facilities that are supported in part by the Hong Kong UGC Special Equipment Grant (SEG HKU09).

REFERENCES

(1) Nugent, W. A.; Mayer, J. M. *Metal-Ligand Multiple Bonds: The Chemistry of Transition Metal Complexes Containing Oxo, Nitrido, Imido, Alkylidene, or Alkylidyne Ligands*; Wiley: New York, 1988.

(2) (a) Schröder, M. Osmium tetraoxide cis hydroxylation of unsaturated substrates. *Chem. Rev.* **1980**, *80*, 187−213. (b) Holm, R. H. Metal-centered oxygen atom transfer reactions. *Chem. Rev.* **1987**, *87*, 1401−1449. (c) Mayer, J. M. Hydrogen atom abstraction by metal-oxo complexes: understanding the analogy with organic radical reactions. *Acc. Chem. Res.* **1998**, *31*, 441−450. (d) Kühn, F. E.; Santos, A. M.; Abrantes, M. Mononuclear organomolybdenum(VI) dioxo complexes: synthesis, reactivity, and catalytic applications. *Chem. Rev.* **2006**, *106*, 2455−2475. (e) Du, G.; Abu-Omar, M. M. Oxo and imido complexes of rhenium and molybdenum in catalytic reductions. *Curr. Org. Chem.* **2008**, *12*, 1185−1198. (f) Gunay, A.; Theopold, K. H. C-H bond activations by metal oxo compounds. *Chem. Rev.* **2010**, *110*, 1060−1081. (g) Yin, G. Active transition metal oxo and hydroxo

DOI: 10.1021/acs.inorgchem.7b02404
Inorg. Chem. XXXX, XXX, XXX−XXX

moieties in nature's redox, enzymes and their synthetic models: structure and reactivity relationships. *Coord. Chem. Rev.* **2010**, *254*, 1826−1842. (h) Piccialli, V. Ruthenium tetroxide and perruthenate chemistry. Recent advances and related transformations mediated by other transition metal oxo-species. *Molecules* **2014**, *19*, 6534−6582. (i) Yam, V. W.-W.; Che, C.-M. Photochemistry and photophysics of trans-d^2-dioxo complexes of osmium(VI). *Coord. Chem. Rev.* **1990**, *97*, 93−104. (j) Lam, W. W. Y.; Man, W.-L.; Lau, T.-C. Mechanisms of oxidation by trans-dioxoruthenium(VI) complexes containing macrocyclic tertiary amine ligands. *Coord. Chem. Rev.* **2007**, *251*, 2238−2252.

(3) (a) Johnson, N. P.; Lock, C. J. L.; Wilkinson, G. Amine, phosphine, arsine, and stilbine complexes of rhenium-(III), -(IV), and -(V). *J. Chem. Soc.* **1964**, 1054−1066. (b) Beard, J. H.; Casey, J.; Murmann, R. K. The preparation and properties of $[Re(amine)_4O_2]^+$ type ions. *Inorg. Chem.* **1965**, *4*, 797−803. (c) Grove, D. E.; Wilkinson, G. Oxo-complexes of rhenium(V). *J. Chem. Soc. A* **1966**, 1224−1230.

(4) (a) Winkler, J. R.; Gray, H. B. Emission spectroscopic properties of dioxorhenium(V) complexes in crystals and solutions. *J. Am. Chem. Soc.* **1983**, *105*, 1373−1374. (b) Winkler, J. R.; Gray, H. B. Electronic absorption and emission spectra of dioxorhenium(V) complexes. Characterization of the luminescent ^3E_g state. *Inorg. Chem.* **1985**, *24*, 346−355. (c) Thorp, H. H.; Van Houten, J.; Gray, H. B. Excited-state properties of dioxorhenium(V). Generation and reactivity of dioxorhenium(VI). *Inorg. Chem.* **1989**, *28*, 889−892.

(5) (a) Pipes, D. W.; Meyer, T. J. Aqueous electrochemistry of *trans*-$(py)_4Re^V(O)_2^+$. Electrocatalytic reductions based on rhenium(II). *J. Am. Chem. Soc.* **1985**, *107*, 7201−7202. (b) Pipes, D. W.; Meyer, T. J. Electrochemistry of trans-dioxo complexes of rhenium(V) in water. *Inorg. Chem.* **1986**, *25*, 3256−3262. (c) Dovletoglou, A.; Adeyemi, S. A.; Lynn, M. H.; Hodgson, D. J.; Meyer, T. J. Novel cis-directed, four-electron dioxo oxidant. *J. Am. Chem. Soc.* **1990**, *112*, 8989−8990. (d) Dovletoglou, A.; Meyer, T. J. Mechanism of cis-directed 4-electron oxidation by a trans-dioxo complex of ruthenium(VI). *J. Am. Chem. Soc.* **1994**, *116*, 215−223.

(6) (a) Che, C.-M.; Lai, T.-F.; Wong, K.-Y. Synthesis, reactivities, and structural studies on high-valent ruthenium oxo complexes. Ruthenium(IV), ruthenium(V), and ruthenium(VI) oxo complexes of tertiary amine ligands. *Inorg. Chem.* **1987**, *26*, 2289−2299. (b) Che, C.-M.; Cheng, W.-K.; Yam, V. W.-W. Syntheses, spectroscopy, and electrochemistry of high-valent osmium(V) and -(VI) oxo complexes of macrocyclic tertiary amine ligands. *J. Chem. Soc., Dalton Trans.* **1990**, 3095−3100. (c) Yam, V. W.-W.; Tam, K.-K.; Cheng, M.-C.; Peng, S.-M.; Wang, Y. Syntheses, spectroscopy and X-ray crystal structures of luminescent nitrido- and trans-dioxo-rhenium(V) complexes of phosphines and arsines. *J. Chem. Soc., Dalton Trans.* **1992**, 1717−1723.

(7) (a) Buchler, J. W.; Smith, P. D. Octaethylporphinato-dioxoosmium(VI): an extreme metal oxidation state within a porphin system. *Angew. Chem., Int. Ed. Engl.* **1974**, *13*, 341−341. (b) Groves, J. T.; Quinn, R. Models of oxidized heme proteins. Preparation and characterization of a trans-dioxoruthenium(VI) porphyrin complex. *Inorg. Chem.* **1984**, *23*, 3844−3846. (c) Che, C.-M.; Chung, W.-C.; Lai, T.-F. Synthesis, reactivity, and X-ray structural characterization of trans-dioxoosmium(VI) porphyrin complexes. *Inorg. Chem.* **1988**, *27*, 2801−2804. (d) Leung, W.-H.; Che, C.-M. High-valent ruthenium-(IV) and -(VI) oxo complexes of octaethylporphyrin. Synthesis, spectroscopy, and reactivities. *J. Am. Chem. Soc.* **1989**, *111*, 8812−8818. (e) Le Maux, P.; Bahri, H.; Simonneaux, G. Preparation, characterization and reaction of the first dioxoruthenium(VI) complexes of chiral picket-fence porphyrins. *J. Chem. Soc., Chem. Commun.* **1994**, 1287−1288. (f) Lai, T.-S.; Zhang, R.; Cheung, K.-K.; Kwong, H.-L.; Che, C.-M. Aerobic enantioselective alkene epoxidation by a chiral trans-dioxo(D_4-porphyrinato)ruthenium(VI) complex. *Chem. Commun.* **1998**, 1583−1584. (g) Göldner, M.; Galich, L.; Cornelissen, U.; Homborg, H. Re^V-phthalocyaninates and Re^V-tetraphenylporphyrinates: synthesis, properties, and crystal structure. *Z. Anorg. Allg. Chem.* **2000**, *626*, 985−995. (h) Jin, N.; Ibrahim, M.; Spiro, T. G.; Groves, J. T. Trans-dioxo manganese(V) porphyrins. *J. Am. Chem. Soc.* **2007**, *129*, 12416−12417.

(8) (a) Kremer, C.; Kremer, E.; Domínguez, S.; Chinea, E.; Mederos, A.; Castiñeiras, A. Synthesis, characterization and potentiometric studies of trans-dioxorhenium(V) complexes. X-ray crystal structure of $[ReO_2(tn)_2]I{\cdot}H_2O$. *Polyhedron* **1996**, *15*, 4341−4347. (b) Kremer, C.; Rivero, M.; Kremer, E.; Suescun, L.; Mombrú, A. W.; Mariezcurrena, R.; Domínguez, S.; Mederos, A.; Midollini, S.; Castiñeiras, A. Synthesis, characterization and crystal structures of rhenium(V) complexes with diphosphines. *Inorg. Chim. Acta* **1999**, *294*, 47−55. (c) Engelbrecht, H. P.; Cutler, C. S.; Jurisson, S. S.; den Drijver, L.; Roodt, A. Solid state study on rhenium dimethylphosphinoethane complexes: X-ray crystal structures of *trans*-$[ReO_2(dmpe)_2]PF_6{\cdot}2H_2O$, *trans*-$[ReO(OH)(dmpe)_2](CF_3SO_3)_2$, *trans*-$[ReN(Cl)(dmpe)_2]$-$CF_3SO_3$ and *trans*-$[ReCl_2(dmpe)_2]ReO_4$. *Synth. React. Inorg., Met.-Org., Nano-Met. Chem.* **2005**, *35*, 83−99. (d) Gancheff, J. S.; Kremer, C.; Ventura, O. N.; Domínguez, S.; Bazzicalupi, C.; Bianchi, A.; Suescun, L.; Mombrú, A. W. ReO_2^+ chelates with aliphatic diamines. Structural and proton transfer properties. *New J. Chem.* **2006**, *30*, 1650−1654.

(9) Iengo, E.; Zangrando, E.; Mestroni, S.; Fronzoni, G.; Stener, M.; Alessio, E. Complexed bridging ligands: oxorhenium(V) compounds with mono-coordinated pyrazine or pyrimidine as possible building blocks for the construction of polynuclear architectures. *J. Chem. Soc., Dalton Trans.* **2001**, 1338−1346.

(10) Royo, B.; Herdtweck, E.; Romão, C. C. Synthesis and structural characterization of novel oxorhenium(V) complexes containing N-heterocyclic carbenes. *Eur. J. Inorg. Chem.* **2004**, *2004*, 3305−3309.

(11) Behling, T.; Capparelli, M. V.; Skapski, A. C.; Wilkinson, G. X-ray crystal structure of the tris(acetato)dioxoosmate(VI) anion. *Polyhedron* **1982**, *1*, 840−841.

(12) (a) Dobson, J. C.; Takeuchi, K. J.; Pipes, D. W.; Geselowitz, D. A.; Meyer, T. J. Redox and spectral properties of the cis and trans isomers of the osmium(VI) dioxo complex $[(bpy)_2Os(O)_2](ClO_4)_2$. *Inorg. Chem.* **1986**, *25*, 2357−2365. (b) Dobson, J. C.; Meyer, T. J. Four-electron oxidations by dioxo complexes of osmium(VI). *Inorg. Chem.* **1989**, *28*, 2013−2016.

(13) Li, C.-K.; Che, C.-M.; Tong, W.-F.; Tang, W.-T.; Wong, K.-Y.; Lai, T.-F. Synthesis, structure, reactivity and electrochemistry of cis-dioxoruthenium-(VI) and -(V) complexes containing *N,N,N′,N′*,3,6-hexamethyl-3,6-diazaoctane-1,8-diamine. *J. Chem. Soc., Dalton Trans.* **1992**, 2109−2116.

(14) (a) Cheng, W.-C.; Yu, W.-Y.; Cheung, K.-K.; Che, C.-M. A novel cis-dioxoruthenium(VI) complex of *N,N′,N″*-trimethyl-1,4,7-triazacyclononane (Me_3tacn) for organic oxidation. *J. Chem. Soc., Chem. Commun.* **1994**, 1063−1064. (b) Che, C.-M.; Yu, W.-Y.; Chan, P.-M.; Cheng, W.-C.; Peng, S.-M.; Lau, K.-C.; Li, W.-K. Alkyne oxidations by cis-dioxoruthenium(VI) complexes. A formal [3 + 2] cycloaddition reaction of alkynes with *cis*-$[(Cn^*)(CF_3CO_2)Ru^{VI}O_2]$-$ClO_4$ (Cn^* = 1,4,7-trimethyl-1,4,7-triazacyclononane). *J. Am. Chem. Soc.* **2000**, *122*, 11380−11392. (c) Yip, W.-P.; Yu, W.-Y.; Zhu, N.; Che, C.-M. Alkene cis-dihydroxylation by $[(Me_3tacn)(CF_3CO_2)Ru^{VI}O_2]$-$ClO_4$ (Me_3tacn = 1,4,7-trimethyl-1,4,7-triazacyclononane): structural characterization of [3 + 2] cycloadducts and kinetic studies. *J. Am. Chem. Soc.* **2005**, *127*, 14239−14249. (d) Chan, S. L.-F.; Kan, Y.-H.; Yip, K.-L.; Huang, J.-S.; Che, C.-M. Ruthenium complexes of 1,4,7-trimethyl-1,4,7-triazacyclononane for atom and group transfer reactions. *Coord. Chem. Rev.* **2011**, *255*, 899−919.

(15) (a) Blackbourn, R. L.; Jones, L. M.; Ram, M. S.; Sabat, M.; Hupp, J. T. Molecular structure of $[(O)_2Re(bpy)(py)_2](ClO_4)_2$: an unusual example of a d^2 metal complex with a cis-dioxo ligand configuration. *Inorg. Chem.* **1990**, *29*, 1791−1792. (b) Ram, M. S.; Johnson, C. S.; Blackbourn, R. L.; Hupp, J. T. Synthesis and electrochemistry of 2,2′-bipyridyl complexes of dioxorhenium(V). *Inorg. Chem.* **1990**, *29*, 238−244. (c) Ram, M. S.; Jones, L. M.; Ward, H. J.; Wong, Y.-H.; Johnson, C. S.; Subramanian, P.; Hupp, J. T. Ligand tuning effects upon the multielectron reduction and single-electron oxidation of (bi)pyridyl complexes of cis- and trans-dioxorhenium(V): redox thermodynamics, preliminary electrochemical kinetics, and charge-transfer absorption spectroscopy. *Inorg. Chem.* **1991**, *30*, 2928−2938.

DOI: 10.1021/acs.inorgchem.7b02404
Inorg. Chem. XXXX, XXX, XXX−XXX

(16) Che, C.-M.; Cheng, J. Y. K.; Cheng, K.-K.; Wong, K.-Y. Reversible proton-coupled Re^{VII}-Re^{VI} and Re^{VI}-Re^{V} couples and crystal structure of $[Re^{V}O_2(OH_2)(Me_3tacn)]BPh_4$ (Me_3tacn = 1,4,7-trimethyl-1,4,7-triazacyclononane). *J. Chem. Soc., Dalton Trans.* **1997**, 2347−2350.
(17) Bandoli, G.; Dolmella, A.; Gerber, T. I. A.; Luzipo, D.; du Preez, J. G. H. Synthesis and structure of the first neutral octahedral cis-dioxorhenium(V) complex. *Inorg. Chim. Acta* **2001**, *325*, 215−219.
(18) (a) Takeuchi, K. J.; Samuels, G. J.; Gersten, S. W.; Gilbert, J. A.; Meyer, T. J. Multiple oxidation states of ruthenium and osmium based on dioxo/diaqua couples. *Inorg. Chem.* **1983**, *22*, 1407−1409. (b) Wong, K.-Y.; Lee, W.-O.; Che, C.-M.; Anson, F. C. Synthesis and electrocatalytic properties of a cis-diaquo-ruthenium(II) complex with 6,6′-dichloro-2,2′-bipyridine. *J. Electroanal. Chem. Interfacial Electrochem.* **1991**, *319*, 207−216.
(19) (a) Odom, A. L.; Mindiola, D. J.; Cummins, C. C. A nucleophilic chromium(V) dioxo radical anion. *Inorg. Chem.* **1999**, *38*, 3290−3295. (b) Tsai, Y.-C.; Wang, P.-Y.; Chen, S.-A.; Chen, J.-M. Inverted-sandwich dichromium(I) complexes supported by two β-diketiminates: a multielectron reductant and syntheses of chromium dioxo and imido. *J. Am. Chem. Soc.* **2007**, *129*, 8066−8067.
(20) (a) Xiao, Z.; Gable, R. W.; Wedd, A. G.; Young, C. G. The cis-dioxomolybdenum(V) radical anion, $[\{HB(Me_2C_2N_3)_3\}MoO_2(SPh)]^-$. *J. Chem. Soc., Chem. Commun.* **1994**, 1295−1296. (b) Xiao, Z.; Gable, R. W.; Wedd, A. G.; Young, C. G. Complexes containing *cis*-$[Mo^{V}O_2]^+$ and *cis*-$[Mo^{V}O(OH)]^{2+}$ centers. *J. Am. Chem. Soc.* **1996**, *118*, 2912−2921. (c) Ng, V. W. L.; Taylor, M. K.; White, J. M.; Young, C. G. cis-Dioxo- and cis-(hydroxo)oxo-Mo(V) complexes stabilized by intramolecular hydrogen-bonding. *Inorg. Chem.* **2010**, *49*, 9460−9469. (d) Young, C. G. Chemical systems modeling the d^1 Mo(V) states of molybdenum enzymes. *J. Inorg. Biochem.* **2016**, *162*, 238−252. (e) Heinze, K. Bioinspired functional analogs of the active site of molybdenum enzymes: intermediates and mechanisms. *Coord. Chem. Rev.* **2015**, *300*, 121−141.
(21) (a) Stravropoulos, P.; Edwards, P. G.; Behling, T.; Wilkinson, G.; Motevalli, M.; Hursthouse, M. B. Oxoaryls of rhenium(V) and -(VI) and osmium(VI). X-ray crystal structures of dimesityldioxorhenium(VI), tetramesityloxorhenium(VI), and dimesityldioxoosmium(VI). *J. Chem. Soc., Dalton Trans.* **1987**, 169−175. (b) Longley, C. J.; Savage, P. D.; Wilkinson, G.; Hussain, B.; Hursthouse, M. B. Alkylimido and oxo aryls of rhenium. X-ray structures of $(Bu^tN)_2ReCl_2(o\text{-}MeC_6H_4)$ and $MO_2(2,6\text{-}Me_2C_6H_3)_2$, M = Re and Os. *Polyhedron* **1988**, *7*, 1079−1088.
(22) DuMez, D. D.; Mayer, J. M. Synthesis and characterization of rhenium(VI) cis-dioxo complexes and examination of their redox chemistry. *Inorg. Chem.* **1998**, *37*, 445−453.
(23) Harms, R. G.; Herrmann, W. A.; Kühn, F. E. Organorhenium dioxides as oxygen transfer systems: synthesis, reactivity, and applications. *Coord. Chem. Rev.* **2015**, *296*, 1−23.
(24) Ciani, G. F.; D'alfonso, G.; Romiti, P. F.; Sironi, A.; Freni, M. Rhenium(V) oxide complexes. Crystal and molecular structures of the compounds *trans*-$ReI_2O(OR)(PPh_3)_2$ (R = Et, Me) and of their hydrolysis derivative $ReIO_2(PPh_3)_2$. *Inorg. Chim. Acta* **1983**, *72*, 29−37.
(25) Felixberger, J. K.; Kuchler, J. G.; Herdtweck, E.; Paciello, R. A.; Herrmann, W. A. Alkyne coordination to organorhenium oxides with rhenium in high oxidation states. *Angew. Chem., Int. Ed. Engl.* **1988**, *27*, 946−948.
(26) (a) Friebe, M.; Jankowsky, R.; Spies, H.; Seichter, W.; Papadopoulos, M.; Chiotellis, E.; Johannsen, B. A mixed-ligand P,S,N-cis-dioxorhenium(V) complex by ligand exchange reactions on trans-monooxo-trichlorobis(triphenylphosphine)rhenium(V): formation and structural studies. *Polyhedron* **1998**, *17*, 3711−3720. (b) Bouziotis, P.; Papagiannopoulou, D.; Pirmettis, I.; Pelecanou, M.; Raptopoulou, C. P.; Stassinopoulou, C. I.; Terzis, A.; Friebe, M.; Spies, H.; Papadopoulos, M.; Chiotellis, E. Synthesis and structural characterization of two cis-dioxorhenium(V) $ReO_2[SN][P]$ mixed-ligand complexes. *Inorg. Chim. Acta* **2001**, *320*, 174−177.
(27) Liu, S.; Senocak, A.; Smeltz, J. L.; Yang, L.; Wegenhart, B.; Yi, J.; Kenttämaa, H. I.; Ison, E. A.; Abu-Omar, M. M. Mechanism of MTO-catalyzed deoxydehydration of diols to alkenes using sacrificial alcohols. *Organometallics* **2013**, *32*, 3210−3219.
(28) Xavier, C.; Paulo, A.; Domingos, A.; Santos, I. Synthesis and structural studies of rhenium(V) complexes stabilized by a monoanionic cyclen ligand. *Eur. J. Inorg. Chem.* **2004**, *2004*, 243−249.
(29) (a) Costas, M.; Tipton, A. K.; Chen, K.; Jo, D.-H.; Que, L., Jr. Modeling rieske dioxygenases: the first example of iron-catalyzed asymmetric cis-dihydroxylation of olefins. *J. Am. Chem. Soc.* **2001**, *123*, 6722−6723. (b) Murphy, A.; Dubois, G.; Stack, T. D. P. Efficient epoxidation of electron-deficient olefins with a cationic manganese complex. *J. Am. Chem. Soc.* **2003**, *125*, 5250−5251. (c) Ottenbacher, R. V.; Bryliakov, K. P.; Talsi, E. P. Nonheme manganese-catalyzed asymmetric oxidation. A lewis acid activation versus oxygen rebound mechanism: evidence for the "third oxidant". *Inorg. Chem.* **2010**, *49*, 8620−8628. (d) Fillol, J. L.; Codolà, Z.; Garcia-Bosch, I.; Gómez, L.; Pla, J. J.; Costas, M. Efficient water oxidation catalysts based on readily available iron coordination complexes. *Nat. Chem.* **2011**, *3*, 807−813. (e) He, Y.; Gorden, J. D.; Goldsmith, C. R. Steric modifications tune the regioselectivity of the alkane oxidation catalyzed by non-heme iron complexes. *Inorg. Chem.* **2011**, *50*, 12651−12660. (f) Klepser, B. M.; Bartlett, B. M. Anchoring a molecular iron catalyst to solar-responsive WO_3 improves the rate and selectivity of photoelectrochemical water oxidation. *J. Am. Chem. Soc.* **2014**, *136*, 1694−1697. (g) Miao, C.; Wang, B.; Wang, Y.; Xia, C.; Lee, Y.-M.; Nam, W.; Sun, W. Proton-promoted and anion-enhanced epoxidation of olefins by hydrogen peroxide in the presence of nonheme manganese catalysts. *J. Am. Chem. Soc.* **2016**, *138*, 936−943. (h) Milan, M.; Bietti, M.; Costas, M. Highly enantioselective oxidation of nonactivated aliphatic C-H bonds with hydrogen peroxide catalyzed by manganese complexes. *ACS Cent. Sci.* **2017**, *3*, 196−204.
(30) (a) Chen, M. S.; White, M. C. A predictably selective aliphatic C-H oxidation reaction for complex molecule synthesis. *Science* **2007**, *318*, 783−787. (b) Suzuki, K.; Oldenburg, P. D.; Que, L., Jr. Iron-catalyzed asymmetric olefin cis-dihydroxylation with 97% enantiomeric excess. *Angew. Chem., Int. Ed.* **2008**, *47*, 1887−1889. (c) Cussó, O.; Garcia-Bosch, I.; Ribas, X.; Lloret-Fillol, J.; Costas, M. Asymmetric epoxidation with H_2O_2 by manipulating the electronic properties of non-heme iron catalysts. *J. Am. Chem. Soc.* **2013**, *135*, 14871−14878. (d) Howell, J. M.; Feng, K.; Clark, J. R.; Trzepkowski, L. J.; White, M. C. Remote oxidation of aliphatic C-H bonds in nitrogen-containing molecules. *J. Am. Chem. Soc.* **2015**, *137*, 14590−14593. (e) Osberger, T. J.; Rogness, D. C.; Kohrt, J. T.; Stepan, A. F.; White, M. C. Oxidative diversification of amino acids and peptides by small-molecule iron catalysis. *Nature* **2016**, *537*, 214−219. (f) Font, D.; Canta, M.; Milan, M.; Cussó, O.; Ribas, X.; Klein Gebbink, R. J. M.; Costas, M. Readily accessible bulky iron catalysts exhibiting site selectivity in the oxidation of steroidal substrates. *Angew. Chem., Int. Ed.* **2016**, *55*, 5776−5779.
(31) (a) England, J.; Britovsek, G. J. P.; Rabadia, N.; White, A. J. P. Ligand topology variations and the importance of ligand field strength in non-heme iron catalyzed oxidations of alkanes. *Inorg. Chem.* **2007**, *46*, 3752−3767. (b) Chow, T. W.-S.; Liu, Y.; Che, C.-M. Practical manganese-catalysed highly enantioselective cis-dihydroxylation of electron-deficient alkenes and detection of a cis-dioxomanganese(V) intermediate by high resolution ESI-MS analysis. *Chem. Commun.* **2011**, *47*, 11204−11206. (c) Hong, S.; Lee, Y.-M.; Cho, K.-B.; Sundaravel, K.; Cho, J.; Kim, M. J.; Shin, W.; Nam, W. Ligand topology effect on the reactivity of a mononuclear nonheme iron(IV)-oxo complex in oxygenation reactions. *J. Am. Chem. Soc.* **2011**, *133*, 11876−11879. (d) Zang, C.; Liu, Y.; Xu, Z.-J.; Tse, C.-W.; Guan, X.; Wei, J.; Huang, J.-S.; Che, C.-M. Highly enantioselective iron-catalyzed cis-dihydroxylation of alkenes with hydrogen peroxide oxidant via an Fe^{III}-OOH reactive intermediate. *Angew. Chem., Int. Ed.* **2016**, *55*, 10253−10257. (e) Shen, D.; Saracini, C.; Lee, Y.-M.; Sun, W.; Fukuzumi, S.; Nam, W. Photocatalytic asymmetric epoxidation of terminal olefins using water as an oxygen source in the presence of a

DOI: 10.1021/acs.inorgchem.7b02404
Inorg. Chem. XXXX, XXX, XXX−XXX

mononuclear non-heme chiral manganese complex. *J. Am. Chem. Soc.* **2016**, *138*, 15857−15860.
(32) Bain, G. A.; Berry, J. F. Diamagnetic corrections and Pascal's constants. *J. Chem. Educ.* **2008**, *85*, 532−536.
(33) Weeks, C. L.; Levina, A.; Dillon, C. T.; Turner, P.; Fenton, R. R.; Lay, P. A. Synthesis and characterization of a chromium(V) cis-dioxo bis(1,10-phenanthroline) complex and crystal and molecular structures of its chromium(III) precursor. *Inorg. Chem.* **2004**, *43*, 7844−7856.
(34) Monillas, W. H.; Yap, G. P. A.; MacAdams, L. A.; Theopold, K. H. Binding and activation of small molecules by three-coordinate Cr(I). *J. Am. Chem. Soc.* **2007**, *129*, 8090−8091.
(35) (a) Lu, K. L.; Lo, H. U.; Lin, Y. C.; Wang, Y. Isomerization, photoreaction, and structure studies of osmium complexes containing carboxamido and halide ligands. *Inorg. Chem.* **1992**, *31*, 4499−4502. (b) Williams, D. S.; Coia, G. M.; Meyer, T. J. Trans-cis isomerization in $[Os(tpy)(Cl)_2(N)]^+$. *Inorg. Chem.* **1995**, *34*, 586−592. (c) Haynes, A.; McNish, J.; Pearson, J. M. Cis−trans isomerism in $[M(CO)_2I_4]^-$ (M = Rh, Ir): kinetic, mechanistic and spectroscopic studies. *J. Organomet. Chem.* **1998**, *551*, 339−347. (d) Bae, B. J.; Park, J. E.; Kim, Y.; Park, J. T.; Suh, I. H. Trans-cis isomerization and structure of $[R_2Ga(\mu\text{-}NHSiEt_3)]_2$ (R = Me, Et). *Organometallics* **1999**, *18*, 2513−2518. (e) Gavriluta, A.; Büchel, G. E.; Freitag, L.; Novitchi, G.; Tommasino, J. B.; Jeanneau, E.; Kuhn, P.-S.; González, L.; Arion, V. B.; Luneau, D. Mechanism elucidation of the cis−trans isomerization of an azole ruthenium−nitrosyl complex and its osmium counterpart. *Inorg. Chem.* **2013**, *52*, 6260−6272.
(36) Lock, C. J. L.; Turner, G. A reinvestigation of dioxobis-(ethylenediamine)rhenium(V) chloride and dioxotetrakis(pyridine)-rhenium(V) chloride dihydrate. *Acta Crystallogr., Sect. B: Struct. Crystallogr. Cryst. Chem.* **1978**, *34*, 923−927.
(37) Dobson, J. C.; Meyer, T. J. Redox properties and ligand loss chemistry in aqua/hydroxo/oxo complexes derived from *cis*- and *trans*-$[(bpy)_2Ru^{II}(OH_2)_2]^{2+}$. *Inorg. Chem.* **1988**, *27*, 3283−3291.
(38) Weinberg, D. R.; Gagliardi, C. J.; Hull, J. F.; Murphy, C. F.; Kent, C. A.; Westlake, B. C.; Paul, A.; Ess, D. H.; McCafferty, D. G.; Meyer, T. J. Proton-coupled electron transfer. *Chem. Rev.* **2012**, *112*, 4016−4093.
(39) Britton, H. T. S.; Robinson, R. A. Universal buffer solutions and the dissociation constant of veronal. *J. Chem. Soc.* **1931**, *0*, 1456−1462.
(40) Verdonck, E.; Vanquickenborne, L. G. Charge-transfer spectra of ruthenium(III)- and osmium(III)-halogenoammine complexes. *Inorg. Chem.* **1974**, *13*, 762−764.
(41) Demachy, I.; Jean, Y. Favoring the cis isomer in d^2 octahedral dioxo complexes: role of the metal. *Inorg. Chem.* **1997**, *36*, 5956−5958.
(42) Demachy, I.; Jean, Y. Trans or (unusual) cis geometry in d^2 octahedral dioxo complexes. A DFT study. *Inorg. Chem.* **1996**, *35*, 5027−5031.
(43) (a) Sawant, S. C.; Wu, X.; Cho, J.; Cho, K.-B.; Kim, S. H.; Seo, M. S.; Lee, Y.-M.; Kubo, M.; Ogura, T.; Shaik, S.; Nam, W. Water as an oxygen source: synthesis, characterization, and reactivity studies of a mononuclear nonheme manganese(IV) oxo complex. *Angew. Chem., Int. Ed.* **2010**, *49*, 8190−8194. (b) Wu, X.; Yang, X.; Lee, Y.-M.; Nam, W.; Sun, L. A nonheme manganese(IV)−oxo species generated in photocatalytic reaction using water as an oxygen source. *Chem. Commun.* **2015**, *51*, 4013−4016.
(44) Chow, T. W.-S.; Wong, E. L.-M.; Guo, Z.; Liu, Y.; Huang, J.-S.; Che, C.-M. cis-Dihydroxylation of alkenes with oxone catalyzed by iron complexes of a macrocyclic tetraaza ligand and reaction mechanism by ESI-MS spectrometry and DFT calculations. *J. Am. Chem. Soc.* **2010**, *132*, 13229−13239.
(45) Sergeeva, E.; Kopilov, J.; Goldberg, I.; Kol, M. 2,2′-Bipyrrolidine versus 1,2-diaminocyclohexane as chiral cores for helically wrapping diamine-diolate ligands. *Inorg. Chem.* **2009**, *48*, 8075−8077.
(46) (a) Jo, D.-H.; Chiou, Y.-M.; Que, L., Jr. Models for extradiol cleaving catechol dioxygenases: syntheses, structures, and reactivities of iron(II)-monoanionic catecholate complexes. *Inorg. Chem.* **2001**, *40*, 3181−3190. (b) Reynolds, M. F.; Costas, M.; Ito, M.; Jo, D. H.; Tipton, A. A.; Whiting, A. K.; Que, L., Jr. 4-Nitrocatechol as a probe of a Mn(II)-dependent extradiol-cleaving catechol dioxygenase (MndD): comparison with relevant Fe(II) and Mn(II) model complexes. *J. Biol. Inorg. Chem.* **2003**, *8*, 263−272.
(47) (a) Bordwell, F. G.; Cheng, J. P.; Harrelson, J. A. Homolytic bond dissociation energies in solution from equilibrium acidity and electrochemical data. *J. Am. Chem. Soc.* **1988**, *110*, 1229−1231. (b) Warren, J. J.; Tronic, T. A.; Mayer, J. M. Thermochemistry of proton-coupled electron transfer reagents and its implications. *Chem. Rev.* **2010**, *110*, 6961−7001.
(48) Gardner, K. A.; Kuehnert, L. L.; Mayer, J. M. Hydrogen atom abstraction by permanganate: oxidations of arylalkanes in organic solvents. *Inorg. Chem.* **1997**, *36*, 2069−2078.
(49) Simmons, E. M.; Hartwig, J. F. On the interpretation of deuterium kinetic isotope effects in C−H bond functionalizations by transition-metal complexes. *Angew. Chem., Int. Ed.* **2012**, *51*, 3066−3072.
(50) Allen, A. D.; Stevens, J. R. Haloammine complexes of osmium(III). *Can. J. Chem.* **1973**, *51*, 92−98.
(51) Brewer, J. C.; Thorp, H. H.; Slagle, K. M.; Brudvig, G. W.; Gray, H. B. Electronic structure of trans-dioxorhenium(VI). *J. Am. Chem. Soc.* **1991**, *113*, 3171−3173.
(52) Luo, Y.-R. *Comprehensive Handbook of Chemical Bond Energies*; CRC Press: Boca Raton, FL, 2007.

DOI: 10.1021/acs.inorgchem.7b02404
Inorg. Chem. XXXX, XXX, XXX−XXX